NASA TECHNICAL NOTE

NASA TN D-5256
c. 1

NASA TN D-5256

A WIND-TUNNEL AND ANALYTICAL STUDY OF THE CONVERSION FROM WING LIFT TO ROTOR LIFT ON A COMPOSITE-LIFT VTOL AIRCRAFT

by Robert J. Huston and James P. Shivers

Langley Research Center
Langley Station, Hampton, Va.

A WIND-TUNNEL AND ANALYTICAL STUDY OF

THE CONVERSION FROM WING LIFT TO ROTOR LIFT ON

A COMPOSITE-LIFT VTOL AIRCRAFT

By Robert J. Huston and James P. Shivers

Langley Research Center
Langley Station, Hampton, Va.

NATIONAL AERONAUTICS AND SPACE ADMINISTRATION

A WIND-TUNNEL AND ANALYTICAL STUDY OF

THE CONVERSION FROM WING LIFT TO ROTOR LIFT ON

A COMPOSITE-LIFT VTOL AIRCRAFT

By Robert J. Huston and James P. Shivers
Langley Research Center

SUMMARY

The principal problem associated with the conversion from wing-borne to rotor-borne flight is the possibility of a large attitude disturbance during the first revolution of the rotor. The aircraft disturbance is due to an oscillation of the lift center of pressure in a longitudinal and lateral direction at a frequency that is simply the number of blades multiplied by the rotor rotational speed.

The results of a wind-tunnel study indicate that large-amplitude cyclic pitch is one means of eliminating the source of the aircraft disturbance for a three-bladed rotor/wing aircraft. In addition, the selection of four blades on a rotor-wing aircraft may so substantially reduce the disturbing moments that cyclic pitch is not required to eliminate the moments.

The results of an analytical investigation indicate that the disturbance may also be reduced in magnitude by a rapid initial rotor acceleration or by the use of an oscillation of the horizontal tail surfaces (elevons) at the frequency of the lift center-of-pressure oscillation. However, simultaneous use of the elevons for longitudinal and lateral control will increase the minimum conversion speeds.

INTRODUCTION

Recent efforts to develop a composite-lift aircraft have been made in an attempt to combine the high hovering efficiency of the helicopter with the high cruise-speed efficiency of the conventional fixed-wing airplane. Most of the composite-lift aircraft are based on independent lift systems, where an attempt can be made to optimize the hovering and cruising lift systems individually.

One system, the rotor/wing, combines the hovering and cruising lift systems into a single lifting surface, a large center hub with three hingeless blades, in an attempt to reduce the weight penalty associated with independent lift systems. For vertical flight

this single lifting surface rotates, whereas for airplane flight the rotor is stopped with one blade forward in the direction of flight.

The purpose of this paper is to examine the aircraft aerodynamics and dynamics that may be encountered with a rotor/wing aircraft during conversion. It has been pointed out (for example, see ref. 1), that the rotor/wing composite-lift aircraft will experience unacceptable attitude disturbances during attempts either to start or stop the rotor if all lift is maintained on the rotor. In this paper the results of wind-tunnel and analytical investigations are used to analyze the motions of this composite-lift aircraft during the conversion. The effect of configuration changes, rotor acceleration rate, and control manipulation are evaluated for the critical phase of the conversion. Portions of this paper were previously published as reference 2.

This paper is organized to describe the concept; summarize the test procedure and results of the NASA wind-tunnel investigations; present an analysis of the aircraft behavior, assuming no attempt at controlling the disturbing moments; and present several methods of reducing either the conversion attitude disturbance or the disturbing moments. The basis of the analysis is presented in appendix A.

SYMBOLS

The physical quantities defined in this section are given in both U.S. Customary Units and the International System of Units (SI). Factors relating the two systems are given in reference 3.

A_0 constant term in expression for θ, hence, mean-blade pitch angle, degrees

A_1 coefficient of $-\cos \psi$ in expression for θ, degrees

A_2 coefficient of $-\cos 2\psi$ in expression for θ, degrees

B_1 coefficient of $-\sin \psi$ in expression for θ, degrees

b wing span, feet (meters)

$C_{cp,X}$ coefficient of $\sin 3\psi$ in expression for lateral center-of-pressure oscillation, defined as $\dfrac{\frac{1}{2} \text{Peak-to-peak rolling moment}}{LR} \times 100$

$C_{cp,Y}$ coefficient of $\cos 3\psi$ in expression for longitudinal center-of-pressure oscillation, defined as $\dfrac{\frac{1}{2}\text{ Peak-to-peak pitching moment}}{LR} \times 100$

C_L lift coefficient, $\dfrac{L}{q_\infty S}$

C_{L_α} rate of change of lift coefficient with angle of attack, per radian

C_l rolling-moment coefficient, $\dfrac{M_X}{q_\infty Sb}$

C_{l_p} damping coefficient due to rolling velocity, $\dfrac{\partial C_l}{\partial\left(\frac{pb}{2V}\right)}$

C_m pitching-moment coefficient, $\dfrac{M_Y}{q_\infty Sc}$.

C_{m_q} damping coefficient due to pitching velocity, $\dfrac{\partial C_m}{\partial\left(\frac{qc}{2V}\right)}$

C_{m_α} rate of change of pitching-moment coefficient with angle of attack, per radian

c wing chord, feet (meters)

D_p damping moment proportional to and opposing aircraft rolling velocity, lbf-ft/rad/sec (N-m/rad/sec)

D_q damping moment proportional to and opposing aircraft pitching velocity, lbf-ft/rad/sec (N-m/rad/sec)

H_p gyroscopic moment proportional to aircraft pitching velocity, lbf-ft/rad/sec (N-m/rad/sec)

H_q gyroscopic moment proportional to aircraft rolling velocity, lbf-ft/rad/sec (N-m/rad/sec)

I_v blade mass moment of inertia about virtual hinge, slug-feet^2 (kilogram-meters^2)

I_X aircraft rolling moment of inertia, slug-feet^2 (kilogram-meters^2)

I_Y aircraft pitching moment of inertia, slug-feet^2 (kilogram-meters^2)

K_α spring moment proportional to and opposing a change in the aircraft pitch attitude, lbf-ft/rad (N-m/rad)

k_X mass radius of gyration of aircraft about X-axis, feet (meters)

k_Y mass radius of gyration of aircraft about Y-axis, feet (meters)

L lift, lbf (N)

$M_{H,A}$ longitudinal rotor-hub moment due to rotation of rotor, lbf-ft (N-m)

$M_{H,B}$ lateral rotor-hub moment due to rotation of rotor, lbf-ft (N-m)

M_X rolling moment, lbf-ft (N-m)

$M_X(t)$ time-variant rolling moment, lbf-ft (N-m)

M_Y pitching moment, lbf-ft (N-m)

$M_Y(t)$ time-variant pitching moment, lbf-ft (N-m)

m mass of aircraft, slugs (kilograms)

N_0 stick-fixed neutral point, percentage of wing chord

p aircraft rolling velocity, radians/second

$\dot{p}$ aircraft rolling acceleration, radians/second^2

q aircraft pitching velocity, radians/second

$\dot{q}$ aircraft pitching acceleration, radians/second^2

q_∞ dynamic pressure, pounds force/foot^2 (newtons/meter^2)

R rotor radius, feet (meters)

S	wing area, feet^2 (meters^2)
t	time, sec
V	velocity, feet/second (meters/second)
x_{cg}	longitudinal location of aircraft center of gravity, percentage of wing chord
α	aircraft angle of attack, degrees
γ_v	blade mass factor (Lock number) based on virtual hinge offset
θ	blade pitch angle at particular azimuth position ψ, $A_0 - A_1 \cos \psi - B_1 \sin \psi - A_2 \cos 2\psi$, degrees
ψ	blade azimuth angle measured from downwind position in direction of rotation, degrees
Ω	rotor angular velocity, radians/second
$\dot{\Omega}$	rotor angular acceleration, radians/second^2
ω_{1R}	cantilever first-flapwise-mode natural frequency of rotating blade, radians/second
ω_{1NR}	cantilever first-flapwise-mode natural frequency of nonrotating blade, radians/second

Subscripts:

des	at design conditions
p	due to rolling velocity
q	due to pitching velocity
$\psi=60$	hub position with reference blade at 60° azimuth position (or other indicated azimuth position)

THE CONCEPT

The rotor/wing configuration under study is shown in figure 1. It combines the hovering and cruising lift systems into a single large hub with three hingeless blades. During vertical or helicopter flight the entire assembly rotates, whereas for airplane flight the rotor is stopped with one blade forward as shown in the figure.

Control

The rotor/wing aircraft uses conventional helicopter and airplane flight controls. The outer 45 percent of the rotor is a hingeless rotor blade with provisions for both collective and cyclic pitch control. Aircraft pitch, roll, and height control are obtained with these controls. Yaw control is obtained with a small fan inserted into the vertical tail surfaces.

Control in airplane flight is obtained from a conventional elevon and rudder arrangement.

Control in autogyro flight and during the conversion is obtained by a combination of the fixed-wing and rotary-wing controls. The controls are interconnected until the rotor is completely stopped.

Conversion

The method of conversion from helicopter to fixed-wing lift is to accelerate the aircraft in the rotary-wing mode to an airspeed above the fixed-wing stall speed and then decelerate the rotor until it stops with one blade forward. The entire conversion procedure from rotor-borne to wing-borne flight is shown in figure 2. The aircraft takes off, hovers, and flies at speeds up to approximately 100 knots in the helicopter mode. At a speed near the maximum obtainable in the helicopter configuration the rotor/wing converts to autorotational flight and a further increase in speed is obtained from the airplane means of propulsion. At a speed greater than the stall speed of the airplane configuration the rotor is slowed, stopped, positioned, and locked in the airplane mode. At speeds above the conversion speed the aircraft flies as a conventional airplane. The procedure is reversed for the wing-borne to rotor-borne conversion. The conversion plan has been documented in detail in reference 4.

MODEL TESTS

Two wind-tunnel investigations were performed at the NASA Langley Research Center to document the characteristics of the rotor/wing composite-lift aircraft. The first investigation was conducted with a powered rotating-wing model. The second

6

investigation, using a nonrotating-wing model, was initiated in an attempt to solve the problems defined in the first investigation. Further details of the model and experimental investigation are included in appendix B.

Rotating-Wing Model

The principle objective of the first investigation was to determine the magnitude of disturbing moments during rotor starts and stops and to determine the effect of variations in the rotor/wing planform on the disturbing moments. The models tested were aerodynamically rigid. Cyclic and collective blade pitch control was provided on the rotors for pitch, roll, and thrust control. For the test results presented in this paper, the models were tested without a horizontal tail. Steady-state aerodynamic characteristics in the helicopter and airplane flight modes, obtained in this investigation, are reported in reference 5.

Test procedure.- The composite-lift conversion was investigated by using two techniques. For both techniques the tunnel velocity was constant. In the first technique, the operating conditions were defined with the model powered at various fixed rotor speeds from 100 percent to 15 percent of the normal rotor speed. In the second technique, the rotor acceleration (increasing rotor speed from zero to normal helicopter rotor speed) and the rotor deceleration (return to zero rotor speed) were made without power to the model.

The first technique was used to determine the zero torque condition which represents the boundary between the rotor accelerating conditions and decelerating conditions. The rotor speed was set, the angle of attack of the model was varied, the collective blade pitch was adjusted to maintain the scale lift, and the model power required was noted. The mean rolling moment was trimmed to zero with cyclic blade pitch although no attempt was made to trim the mean pitching moment to zero since it was assumed that the horizontal tail surface would provide the necessary trim control. Based on these data, a schedule of the model angle of attack, collective blade pitch, and cyclic blade pitch as a function of rotor speed was obtained for the conversion.

In the second technique, unpowered conversions were performed by using the boundary determined from the powered conversions. The model angle of attack, collective blade pitch, and cyclic blade pitch were manually adjusted by noting the actual rotor speed and adjusting the controls to match the predetermined schedule. A separate operator was assigned to each control.

The initial or final conditions (i.e., the 0-rpm condition) for all conversions were the conditions of zero cyclic and collective blade pitch. The rotor acceleration was initiated by lowering the collective blade pitch from zero to negative angles to produce an accelerating torque on the rotor. The rotor deceleration was initiated by setting a large positive

collective pitch to produce a decelerating torque on the rotor. As the rotor speed approached zero, the collective pitch was reduced to or near zero as the rotor stopped.

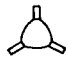More specific details of the complete conversion are included in appendix B.

Test results.- The most significant characteristic observed during the conversion was an oscillation of the lift center of pressure both longitudinally and laterally, at a frequency equal to the number of blades times the rotor rotational speed. A typical time history of this oscillation during a rotor start and rotor stop is shown in figure 3. The oscillation is the predominant characteristic found throughout the rotor speed range during the unpowered conversions. A mean longitudinal trim shift equal to one-half of the peak-to-peak amplitude of the longitudinal moment oscillation is also evident. There was no significant variation in the mean lift at constant angle of attack during the low-rotor-speed portion of the rotor start or stop.

The longitudinal and lateral oscillations of the lift center of pressure are due to the rotation of the center of lift in an elliptical path on the rotor hub as illustrated in figure 4. The instantaneous location of the center of lift is plotted on the rotor/wing planform for azimuth positions corresponding to one-third of a revolution of the rotor. The blade to which the azimuth notation refers is shaded. The $\psi = 60^\circ$ position corresponds to the wing position for airplane flight. The line indicates the path the lift center of pressure follows, while the heavy point indicates the instantaneous location of the center of lift. Because of the symmetry of the model, the center-of-pressure variation repeats itself three times during each revolution.

There was no significant difference in the amplitude of the center-of-pressure oscillation due to varying the planform of the three-bladed hub. The initial and final amplitudes of the pitching- and rolling-moment oscillations for three rotor/wing planforms are shown in table I. The peak-to-peak values of the pitching and rolling moments are presented as a lift center-of-pressure fluctuation in percent of the rotor radius. The data which were obtained from seven rotor-start and rotor-stop cycles indicate that there is no clear advantage between configurations on the basis of the variation of longitudinal or lateral lift center of pressure during the first revolution.

Preliminary calculations, based on the test results obtained with the rotating-wing model, indicated that any significant attitude disturbances from the center-of-pressure oscillation would occur at rotor speeds of about 15 percent of the normal helicopter rotor speed. At such low rotor speeds the phase angle of forced response was determined to be considerably less than 20° of blade azimuth, which suggests that methods of center-of-pressure control could be studied with static models. Based on these conclusions, the second wind-tunnel investigation was initiated.

TABLE I.- CENTER-OF-PRESSURE OSCILLATION

Rotor configuration		$2\,C_{cp,Y}$, % of R	$2\,C_{cp,X}$, % of R	$\dfrac{\text{Mean lift}}{q_\infty \pi R^2}$	α, deg
During first revolution of rotor start					
1		23	12	0.22	14.4
2		25	15	0.22	14.9
		22	13	.21	14.9
		22	15	.23	15.8
		20	13	.22	15.9
3		26	13	0.18	15.5
		30	12	.18	15.7
During last revolution of rotor stop					
1		25	15	0.18	11.4
2		27	14	0.19	12.7
		24	14	.22	15.9
		31	13	.23	15.8
3		27	10	0.16	14.3
		33	15	.17	14.3

Nonrotating-Wing Model

The objective of the second wind-tunnel investigation was to determine what mechanism could be used to control the lift center of pressure during a "rotation" of the rotor/wing. The results for a nonrotating-wing model indicate that blade cyclic pitch on a three-blade configuration will minimize lift center-of-pressure movement and that there is no significant center-of-pressure motion on a four-blade configuration.

The test technique utilized to investigate the conversion of this composite-lift configuration was to successively rotate and lock the wing in various azimuth positions. At each new blade azimuth position the forces and moments were measured for an angle-of-attack range. With a set of successive rotations of the rotor, the static variation of

forces and moments could be obtained which corresponded to that experienced by a very slowly rotating rotor.

The models tested had flat-plate three- and four-blade rotor/wing planforms. Both planforms had the same ratio of blade span to blade radius. During most of the tests with the three-blade configuration the blade pitch was scheduled with azimuth position in an attempt to eliminate lift center-of-pressure movement as a function of azimuth position. The blade pitch angle schedule corresponds to conventional helicopter first-harmonic cyclic pitch.

Center-of-pressure movement on three-blade rotor.- The effect of large-amplitude blade cyclic pitch on the lift center-of-pressure movement during one-third of a rotor revolution is shown in figure 5 for constant angle of attack. The data presented are for a blade pitch input of $\theta = 0$ and for $\theta = -30 \sin \psi$. Zero blade cyclic pitch is seen to produce essentially the same three-per-rotor-revolution oscillation as previously measured during actual rotor starts and stops and shown in figure 3. For the case with which the cyclic pitch was used, however, the longitudinal variation of the center of pressure during the rotor revolution was greatly reduced and the lateral variation of the center of pressure was reduced and reversed. The significant reduction in the longitudinal center-of-pressure oscillation and the reversal and reduction of the lateral center-of-pressure oscillation suggests that an acceptable center-of-pressure oscillation can be obtained at other angles of attack.

The amplitude of the blade cyclic pitch required to reduce the lift center-of-pressure oscillations is reduced at lower angles of attack of the aircraft. The effect of angle of attack and blade cyclic pitch on the peak-to-peak moments due to the lift center-of-pressure oscillations is shown in figure 6. In this figure, the referenced azimuth angles, at which the peak-to-peak moments are compared, were chosen from figure 5 for the case of $\theta = 0$. This presentation avoids confusion by ignoring both slight shifts in the azimuth angle of peaks and multiple peaks in a cycle. Both of these phenomena are illustrated in figure 5 for $\theta = -30 \sin \psi$ and are typical of the data used to prepare figure 6.

The pitching- and rolling-moment coefficients of figure 6 are proportional to the product of the lift coefficient C_L and the nondimensional center-of-pressure coefficient $C_{cp,X}$ or $C_{cp,Y}$. All the data presented were obtained at lift coefficients below the maximum (see fig. 7) and in a region showing only a gradual decrease in the lift-curve slope with an increase in angle of attack. Therefore, a variation of the peak-to-peak moments with angle of attack that resembles a lift curve, as does the $\theta = 0$ curve at low angles of attack, indicates a center-of-pressure coefficient (the amplitude of the center-of-pressure motion during a rotor revolution) that is unaffected by angle of attack.

10

At angles of attack above about 12° and 10° for the pitching and rolling moments, respectively, the peak-to-peak moments of figure 6 indicate that local stall or separation reduced the center-of-pressure motion for $\theta = 0$. That is, since the lift is still increasing with angle of attack, the constant or decreasing moment coefficients indicate a redistribution of lift. For $\theta = -15 \sin \psi$, the center-of-pressure motion is reversed at low angles of attack (as typically illustrated in figure 5), becomes zero at 5° and 7° angle of attack and builds to a maximum at 16° and 20° angle of attack for pitch and roll, respectively. Above the angle of attack for maximum moment, the center-of-pressure motion is limited by local stall and separation.

An increase in the rotor/wing thickness and blade camber would be expected to result in a change in the angle of attack for zero center-of-pressure oscillation (at constant blade cyclic pitch) and a further increase in the maximum peak-to-peak moment coefficients that are presently limited by flow separation or stall. Consideration of all effects suggests that the lift center-of-pressure oscillation during conversion may be less of a problem at higher conversion airspeeds where, because of the lower angles of attack, considerably smaller cyclic pitch inputs may be required to reduce the center-of-pressure oscillation.

Lift penalty with three-blade rotor.- A lift penalty is associated with the requirement for large-amplitude cyclic pitch at high rotor/wing angles of attack to reduce the rotor/wing center-of-pressure oscillations to an acceptable magnitude. The variation of lift coefficient with angle of attack with and without cyclic blade pitch is presented in figure 7. The solid and broken lines indicate the lift coefficient of the nonrotating wing ($\psi = 60^O$) with and without cyclic blade pitch, respectively. The dotted area indicates the amplitude of the lift-coefficient oscillations during a rotor revolution for zero cyclic pitch, and the lined area indicates the amplitude of the lift-coefficient oscillations for 30° of cyclic blade pitch. For the range of interest, the mean lift coefficient is reduced approximately one-tenth by the introduction of large-amplitude cyclic pitch to reduce the center-of-pressure oscillation; however, the amplitude of the lift oscillation is reduced. Generally, at constant angle of attack, the lift oscillation would result in approximately a $\pm\frac{1}{10}$g vertical oscillation of the aircraft at the frequency of 3 times the rotor speed.

Effect of number of blades.- The selection of four blades on this composite-lift design may completely eliminate any concern for aircraft motions due to the lift center-of-pressure oscillation. The effect of the number of blades on the magnitude of the peak-to-peak moments during a rotor revolution is shown in figure 8. The models had the same diameter, but the effective solidity and wing area of the four-blade rotor/wing is substantially increased for the test model. Examination of the data for the four-blade configuration indicates that the longitudinal center-of-pressure oscillation is about ±2percent of the rotor radius and that the lateral center-of-pressure oscillation is about

±0.75 percent of the rotor radius at an angle of attack of 12°. Since the four-blade configuration was arbitrarily chosen and may not be an optimum shape, these results indicate that further efforts to define an ideal rotor/wing shape may prove fruitful.

ANALYSIS OF AIRCRAFT BEHAVIOR DURING CONVERSION

The effect of a lift center-of-pressure oscillation during conversion is shown to produce a large pitch and roll attitude disturbance during the first or last revolution of the rotor. The amplitude of the disturbance is proportional to the magnitude of the lift and the amplitude of the lift center-of-pressure oscillation.

In order to evaluate the significance of the lift center-of-pressure oscillation, a two-degree-of-freedom analysis was made of the motions of a typical three-blade composite-lift aircraft. The physical and aerodynamic characteristics are those of a proposed vehicle with a design gross weight of 19 635 lbf (87 336 N), a wing loading of 37.3 lbf/ft^2 (1786 N/m^2), an airplane span of 45 ft (13.7 m), and a rotor diameter of 50 ft (15.24 m). The helicopter controls are designed to provide satisfactory helicopter flying qualities based on the specifications of reference 6 (MIL-H-8501A). The size of the fixed and movable airplane control surfaces are designed to provide satisfactory airplane flying qualities based on the specifications of reference 7 (MIL-F-8785 (ASG)). For the analysis the three-per-revolution lift center-of-pressure oscillation was assumed to be of constant magnitude and phasing during the rotor start for rotor speeds from 0 to 40 percent of the normal rotor speed. The analytical method contained in appendix A can be applied to any number of blades.

Pitch Attitude Disturbance

An initial pitch attitude change of 0.10 radian is shown to occur during the first two-thirds of a revolution of a rotor start with this composite-lift aircraft. A time history of the calculated longitudinal response of this composite-lift aircraft is presented in figure 9 for a rotor start at an airspeed of 150 knots. For the case presented, it was assumed that the longitudinal three-per-revolution center-of-pressure oscillation had a peak-to-peak amplitude of 25 percent of the rotor radius $\left(C_{cp,Y} = 12.5\right)$ and the lateral oscillation had a peak-to-peak amplitude of 12.5 percent of the rotor radius $\left(C_{cp,X} = 6.25\right)$. The airplane damping in pitch and roll were augmented by additional rotor damping and gyroscopic terms proportional to rotor speed. A longitudinal trim change equal to one-half of the peak-to-peak pitching moment was considered to have been applied by the elevator control in order to retrim the mean pitching moments on the aircraft to zero during the first half-revolution. Based on a calculation of the angular acceleration of the rotor during an autorotation start, the rotor angular acceleration was assumed to be constant at 3.2 rad/sec^2.

The peak pitch attitude disturbance of 0.10 radian occurs simultaneously with completion of the first two-thirds of a revolution of the rotor. At the assumed rotor acceleration, the first two-thirds of a revolution of the rotor is obtained in 1.62 sec. After the initial spike, the amplitude of the pitch-rate oscillations reduces with increasing rotor speed and results in little further attitude change. The pitch attitude, after the initial disturbance, returns toward the initial trim point under the influence of the aircraft static stability.

Roll Attitude Disturbance

An initial roll attitude change of 0.20 radian will occur at completion of one-quarter of a revolution of a rotor start with this composite-lift aircraft. The time history of the calculated lateral response during a rotor start is presented in figure 10. The same conditions and assumptions apply to the lateral response as were applied to the longitudinal response. After the initial roll-rate spike, the amplitude of the roll-rate oscillations reduces with increasing rotor speed and effects the roll attitude very little. The subsequent roll attitude drift is due to the increasing magnitude of the assumed gyroscopic moment coupled to the mean nose-down pitching velocity.

Significance of Results of Analysis

The only significant attitude disturbance, due to the lift center-of-pressure oscillation, occurs during the first rotor revolution of the accelerating conversion. A similar effect can be anticipated during the last rotor revolution of a decelerating conversion. The rotor speed at the time of the attitude disturbance is below 20 percent of the normal rotor speed, where the effects of rotation on the aerodynamic load distribution and the structural dynamic response are believed to be small.

CONTROL OF THE ATTITUDE DISTURBANCE

Attitude disturbances can be reduced in magnitude or possibly eliminated by the use of blade cyclic pitch, the use of a four-blade instead of a three-blade configuration, the use of oscillating elevon deflection, or the use of high rotor angular acceleration and deceleration. Simply accepting an attitude disturbance during conversion is not believed to be practical. From an operational viewpoint, the aircraft should have reasonable maneuver freedom at any point in the conversion. The use of methods to control the lift center-of-pressure position or to counter the resulting pitch and roll moments will prevent a rigid conversion technique from being required. Each of the following possible approaches to prevent a large attitude disturbance must be evaluated by the designer.

Blade Cyclic Pitch

The use of blade cyclic pitch was shown in figure 6 to provide a positive control of the amplitude of both the longitudinal and lateral motions of the lift center of pressure. Some automatic device, operating as a function of rotor speed and angle of attack, might be developed to control the amplitude and phasing of the blade cyclic angle and to return the cyclic pitch control to the pilot for helicopter flight.

Four-Blade Rotor/Wing

The use of a four-blade composite-lift configuration was shown in figure 8 to provide a substantial reduction in the lift center-of-pressure oscillations without the use of blade cyclic pitch. The results with the four-blade configuration examined do indicate that further efforts to define an ideal composite-lift planform may prove fruitful.

Elevon Control

The elevons may be used to counter the pitching and rolling moments produced by the lift center-of-pressure oscillation. The longitudinal and lateral control capability of the aircraft assumed for analysis is adequate for trim above 142 knots.

Longitudinal control.- The elevon control moment available from the horizontal tail as a function of the airspeed is presented in figure 11. Included is the required moment to balance the longitudinal trim shift and the most nose-up moment during the rotor start. The required moments are based on the assumption that the amplitude of the longitudinal center-of-pressure oscillation was constant throughout the speed range. Since the available longitudinal control is capable of trimming the moments due to the longitudinal center-of-pressure oscillation, there is some control margin available for maneuver requirements. That is, it is possible to eliminate the oscillatory longitudinal response during the rotor start by using a pitch oscillation of the horizontal tail and still retain some maneuver margin.

The initial pitch attitude disturbance might be controlled by a single pitch motion of the elevons; however, vibrational inputs subsequent to the first revolution of the rotor may be too extreme for passenger comfort. Therefore, it appears reasonable to require a pitch oscillation of the elevons during the rotor start for rotor speeds from 0 to 20 percent of the normal helicopter rotor speed.

The horizontal tail deflections required to trim the rotor/wing pitching moments completely during a rotor start up to 20 percent of normal rotor speed are presented in figure 12, assuming no time lag between the control input and the control moment. If the horizontal tail oscillation is stopped at the end of the second rotor revolution, as shown, the longitudinal center-of-pressure oscillation would then result in about a ±0.025 rad/sec

pitching-velocity oscillation of the aircraft. (See fig. 9.) The aircraft pitch attitude changes associated with these pitching velocities would then be negligible.

Control of the horizontal tail oscillations required to counter the longitudinal center-of-pressure oscillation may be an extremely taxing design problem. An automatic device would appear to be necessary in that, if control is attempted manually, the pilot could get out of phase and cause an aircraft upset.

Lateral control.- The lateral control moment available is adequate to trim the lateral center-of-pressure oscillation above an airspeed of 143 knots. The lateral control moment available and that required to trim the lateral center-of-pressure oscillation is presented in figure 13. The available control is based on the assumption that the elevons are differentially deflected to 30° with no requirement for roll control due to yaw or for loss of roll effectiveness due to elevator deflection. There is no margin for maneuvering at this speed. Simultaneous use of the elevons for longitudinal and lateral trim of the center-of-pressure oscillation and for maneuvering will increase the minimum conversion speed above 143 knots.

Rotor Angular Acceleration

The rate of acceleration of the rotor is a powerful tool in reducing the amplitude of the attitude disturbance when no attempt is made to control the center-of-pressure oscillations. The effect of rotor angular acceleration on the disturbance amplitude is presented in figure 14. The attitude peak is presented as the ratio of the peak to the corresponding center-of-pressure coefficient. This presentation is possible because the assumptions of the analysis lead to a linear relationship between the attitude peak and the center-of-pressure coefficient, It would appear, based on a comparison of figures 9, 10, and 14, that a high acceleration rate would only be necessary during the critical 2 sec of the rotor start. A similar conclusion can be inferred for a rotor stop, that a high deceleration during the critical seconds would help to minimize the attitude disturbance problem. The effect of angular acceleration on the disturbance amplitude and the requirement for indexing the blades at a given position suggest that a precise and powerful rotor-speed control mechanism is required during conversion.

Aeroelastic Effects

The analysis of aircraft motions due to the lift center-of-pressure motion and the choice of methods of control of the attitude disturbance are based on data from rigid models. It appears that blade and hub bending due to aeroelastic effects may increase the amplitude of the center-of-pressure motion and further aggravate the attitude disturbance problem during conversion. The possibility of larger amplitude center-of-pressure

motion, when aeroelastic effects are considered, suggests that solutions which attempt to control the center-of-pressure motion should be favored.

CONCLUDING REMARKS

The data, analysis, and discussion contained in this paper provide a basis for determining the direction in which future research on the rotor/wing aircraft may proceed. The material presented is not intended to provide a final solution to the problems encountered in conversion from wing-borne to rotor-borne flight with the rotor/wing aircraft. The aeroelastic problems associated with the conversion must also be considered. Although such a treatment is not attempted in this paper, examination of solutions to the attitude disturbance problems should not be considered complete without considering the effect of the solutions on the aeroelastic problems.

On the basis of the data and analysis included in this paper, the following conclusions may be drawn:

1. The principal problem associated with the conversion from wing-borne to rotor-borne flight of a three-blade rotor/wing is the possibility of a large attitude disturbance during the first revolution of the rotor.

2. The aircraft disturbances are due to a rotation of the lift center of pressure in an elliptical path at a frequency that is simply the number of blades times the rotational speed.

3. The moments causing the longitudinal and lateral disturbance of a three-blade rotor/wing can be trimmed by an oscillation of the horizontal tail surface (elevons); however, simultaneous use of the elevons for trim and maneuvers will increase the minimum conversion speeds.

4. Large-amplitude cyclic pitch is one means of eliminating the source of the aircraft disturbance on a three-blade configuration.

5. The adoption of a four-blade configuration on a rotor/wing aircraft may result in sufficiently small disturbing moments during the start or stop that concern for an attitude disturbance will be eliminated.

Langley Research Center,
    National Aeronautics and Space Administration,
        Langley Station, Hampton, Va., March 20, 1969,
            721-01-00-36-23.

APPENDIX A

CONVERSION ANALYSIS METHOD, ASSUMPTIONS,
AND EFFECT OF ASSUMPTIONS

ANALYSIS[1]

An analysis of the significance of the oscillatory moments was made by considering the two-degree-of-freedom response of a typical three-blade rotor/wing aircraft to a rotation of the lift center of pressure at 3 times the rotor speed. Initially assuming no elevon or other control moments to counter the oscillations, the pitching- and rolling-moment forcing functions were written

$$M_Y(t) = \frac{LR\left(C_{cp,Y}\right)}{100}(1 + \cos 3\psi) \tag{1}$$

$$M_X(t) = \frac{LR\left(C_{cp,X}\right)}{100}(+\sin 3\psi) \tag{2}$$

The azimuth angle may be represented, for constant angular acceleration, by the following equation:

$$\psi = \frac{\pi}{3} + \frac{1}{2}\Omega t \tag{3}$$

Therefore, equations (1) and (2) can be written

$$M_Y(t) = \frac{LR\left(C_{cp,Y}\right)}{100}\left(1 - \cos\frac{3\Omega t}{2}\right) \tag{4}$$

$$M_X(t) = \frac{LR\left(C_{cp,X}\right)}{100}\left(-\sin\frac{3\Omega t}{2}\right) \tag{5}$$

---

[1]The analysis of reference 2 includes several errors in the statement of the equations. These errors have been corrected in the present paper. The only significant result of these errors was to present incorrect values of rotor acceleration and rotor speed in the calculated aircraft response characteristics. The time history of calculated disturbances is unchanged.

APPENDIX A

Constant angular acceleration of the rotor (about the shaft axis) was assumed, therefore

$$\Omega = \dot{\Omega}t \tag{6}$$

Substituting equation (6) into equations (4) and (5) gives

$$M_Y(t) = \frac{LR\left(C_{cp,Y}\right)}{100}\left(1 - \cos\frac{3\dot{\Omega}t^2}{2}\right) \tag{7}$$

$$M_X(t) = -\frac{LR\left(C_{cp,X}\right)}{100}\left(\sin\frac{3\dot{\Omega}t^2}{2}\right) \tag{8}$$

Because there is a mean longitudinal trim shift when the rotor is started, a term to retrim the pitching moment can be added to the parenthetical term in equation (7). It was assumed that 95 percent of this moment would be introduced during approximately the first half-revolution (3 radians) of the rotor. The expression to be added to equation (7) is

$$-\frac{LR\left(C_{cp,Y}\right)}{100}\left(1 - e^{-\Omega t/2}\right)$$

Substituting equation (6) into this expression and adding the resultant expression to equation (7) gives

$$M_Y(t) = \frac{LR\left(C_{cp,Y}\right)}{100}\left(e^{-\dot{\Omega}t^2/2} - \cos\frac{3\dot{\Omega}t^2}{2}\right) \tag{9}$$

The two-degree-of-freedom equations of motion used for the analysis were

$$\dot{q} + \frac{D_q}{I_Y}q + \frac{K_\alpha}{I_Y}\int_0^t q\,dt + \frac{H_q}{I_Y}p = \frac{M_Y(t)}{I_Y} \tag{10}$$

$$\dot{p} + \frac{D_p}{I_X}p - \frac{H_p}{I_X}q = \frac{M_X(t)}{I_X} \tag{11}$$

The damping, gyroscopic cross coupling, and static stability margin were expressed in terms of the airspeed and the rotor speed. The values of these stability derivatives and the dimensional quantities of the aircraft under analysis are as follows:

18

APPENDIX A

(1) Damping in pitch:

    (a) Contribution due to tail

$$\left(C_{m_q}\right)_{tail} = -9.44$$

    (b) Contribution due to rotation of rotor[2]

$$\left[\Delta\left(\frac{M_{H,A}}{I_V\Omega}\right)_q\right]_{rotor} = -0.48$$

    (c) Total damping in pitch per sec[3]

$$\frac{D_q}{I_Y} = \frac{3000\dot{\Omega}Et + 740V}{mk_Y^2}$$

(2) Damping in roll:

    (a) Contribution due to rotor/wing-tail combination[4]

$$\left(C_{l_p}\right)_{rotor/wing\text{-}tail} = -0.25$$

    (b) Contribution due to rotation of rotor[2]

$$\left[\Delta\left(\frac{M_{H,B}}{I_V\Omega}\right)_p\right]_{rotor} = -0.48$$

    (c) Total damping in roll per sec

$$\frac{D_p}{I_X} = \frac{3000\dot{\Omega}Et + 160V}{mk_X^2}$$

---

[2]Rotor stability derivatives are based on the analysis of reference 8 for $\omega_{1NR}/\Omega_{des} = 1$, $\omega_{1R}/\Omega_{des} = 1.5$, and $\gamma_V = 3$.

[3]The coefficient E was introduced as an artificial multiplier of the moment contributions due to rotation of the rotor in order that their effect on the calculated response could be determined. For the moment contribution in the terms in items 1(b), 2(b), and 3(b), the coefficient E was set equal to 1.0. In order to eliminate any moment contribution due to rotation of the rotor, the coefficient was set equal to 0.

[4]The roll damping is based on stability derivatives obtained with the nonrotating model described in this paper with the blades in the $\psi = 60°$ orientation.

APPENDIX A

(3) Rotor gyroscopic moment:[2]

(a)
$$\left[\Delta\left(\frac{M_{H,B}}{I_V\Omega}\right)_q\right]_{rotor} = -\left[\Delta\left(\frac{M_{H,A}}{I_V\Omega}\right)_p\right]_{rotor} = 1.44$$

(b) Gyroscopic moment[3]

$$\frac{H_q}{I_Y} = \frac{9000\dot{\Omega}Et}{mk_Y^2} \qquad\qquad \frac{H_p}{I_X} = \frac{9000\dot{\Omega}Et}{mk_X^2}$$

(4) Longitudinal static stability

$$C_{m_\alpha} = C_{L_\alpha}\left(x_{cg} - N_0\right) = 2.86\left(x_{cg} - N_0\right)$$

therefore

$$\frac{K_\alpha}{I_Y} = \frac{26V^2\left(x_{cg} - N_0\right)}{mk_Y^2}$$

ROTOR/WING DIMENSIONAL QUANTITIES ASSUMED FOR ANALYSIS

Rotor radius . . . . 25 ft (7.62 m)

Wing area . . . . $0.268\pi R^2$

Wing mean aerodynamic chord 0.63R

Wing span 1.8R

Roll radius of gyration, k_X 0.203R

Pitch radius of gyration, k_Y 0.63R

Rotor polar radius of gyration 0.48R

Rotor weight . . . . 0.14 design gross weight

Design disk loading . . . . 10 lbf/ft^2 (478.8 N/m^2)

Horizontal tail length 1.2R

Horizontal tail span 1.12R

Horizontal tail area . . . . $0.094\pi R^2$

Design rotor speed . . . . 28.8 rad/sec

---

[2]See footnote 2 on page 19.

[3]See footnote 3 on page 19.

APPENDIX A

EFFECT OF CONVERSION VELOCITY

The effect of the aircraft velocity on the disturbance amplitudes is presented in figure 15. For a direct comparison, the ordinate scales of figures 14 and 15 are the same. It is seen that a substantial increase in the airspeed is necessary to reduce the amplitude of the attitude disturbance. Also, the increased dynamic pressure would cause even the reduced attitudes at higher conversion speeds to produce higher vertical accelerations of the aircraft.

EFFECT OF STATIC MARGIN AND ROTOR MOMENTS

The effect of the aircraft static margin and the magnitude of the assumed rotor angular velocity moments is presented in figure 16. Increasing the static margin is seen to be a relatively ineffective method of reducing the amplitude of the attitude disturbance.

The assumed angular velocity damping and gyroscopic moments very slightly increase the amplitude of the pitch attitude disturbance. It appears that the gyroscopic coupling is producing the predominant effect. However, because of the very slight effect and the uncertainty in the magnitude of the damping values, it appears reasonable to consider the attitude disturbance problem as uncoupled; that is, in future analysis of the conversion, the lateral-directional response can be considered separately from the complete longitudinal response.

APPENDIX B

STEADY-STATE AERODYNAMIC CHARACTERISTICS
DURING CONVERSION

In previous sections of this paper, attention has been concentrated on the dynamics of the airframe during the low-rotor-speed portion of the conversion from airplane flight to helicopter flight. In this section, the steady-state aerodynamic characteristics during the conversions are presented. In addition, a limited description of the model and instrumentation is included.

MODEL

Drawings of the model are given in figure 17, and a photograph of the model mounted in the Langley full-scale tunnel is given as figure 18.

The fuselage was a wood-covered aluminum box. The rotor support structure and the drive and control mechanisms were located inside the fuselage. The aft fuselage section was fitted with a vertical tail and included provisions for a variable-incidence horizontal tail. Only the characteristics for the model with the horizontal tail off, however, are included herein.

Sketches of the three rotor/wing planforms and details of the cross sections are given in figures 19, 20, and 21. All planforms were of equal diameter. The hub of configuration 1 had convex curvature between the three constant-chord blades, configuration 2 had a straight-sided hub connecting three tapered blades, and configuration 3 had a concave curvature between three tapered blades. Consequently, the surface area of each configuration was different. The hub portion of each rotor/wing was made of mahogany covered with fiber glass. The blades were balsa wood covered with fiber glass and fitted over metal ribs and spars. The blades were composed of biconvex sections with parabolic leading and trailing edges. These sections were symmetrical about both the chord line and the midchord point. The blades were attached to the hub through feathering bearings; no flapping hinges were provided.

The rotors were shaft driven in the helicopter model by a hydraulic motor and pump arrangement through a roller chain transmission. Rotor speed was controlled by varying the hydraulic pressure at the pump.

Rotor cyclic and collective pitch were accomplished through a swash-plate system, the upper part of which was connected to each blade by rigid links. The swash plate had a wave built into it so that it provided 2.5^O of second-harmonic cyclic pitch A_2 during

each revolution. The cyclic pitch range available was between 16° and -16°, and the collective pitch range was from -11° to 21.5°.

The model was mounted on a pedestal that was fixed to the ground plane so that the rotor/wing was located approximately on the tunnel center line 13 feet above the ground board. A six-component strain-gage balance was attached between the top of the pedestal and the model so that it rotated with the model in the longitudinal plane as shown in figure 22. The angle of attack of the model was varied by an electric actuator through an available range from about -15° to 20°. Additional details of the model are included in reference 5.

INSTRUMENTATION

The forces and moments on the model were sensed by the six-component strain-gage balance. The model angle of attack and rotor control positions were sensed by potentiometers, and rotor speed was measured by a tachometer.

The output signals from the angle-of-attack, control-position, and rotor-speed sensors were fed to an operator's console which provided visual indication of the model operating conditions and included provisions for varying these conditions. The signals provided at the control console along with the outputs from the balance and a magnetic azimuth-position pickup were recorded on an oscillograph. Also, the signals from the balance, the angle-of-attack sensor, and the tunnel static-pressure sensor were electrically fed into a digital readout and tape-recording system. Other pertinent quantities such as rotor speed, control positions, air density, and hydraulic pressure differential across the balance were manually inserted into the digital tape system.

TEST RESULTS

A number of conversions from airplane flight to helicopter flight and return were made with each configuration investigated and the aerodynamic characteristics for two typical conversions for each configuration are presented. The conversion results are subdivided into two categories: (a) complete autorotation conversion and (b) abbreviated autorotation conversions. The data presented in figures 23 to 26 (complete autorotation conversions) are for conversions with configurations 1, 2, and 3 in which the rotor speed was controlled aerodynamically from 0 to approximately 500 rpm with a subsequent controlled reduction in the rotor speed to 0 rpm. The data in figures 23 to 26 include the model angle of attack α, rotor collective and cyclic blade pitch angles A_0, A_1, B_1, and A_2, and the variation in the nondimensional steady forces and moments as a function of the rotor speed. A time history of the rotor speed is also included. The force and

moments presented were obtained from the oscillograph records and were limited to the measurement of the change in force and moment from the initial or final 0-rpm condition.

The data presented in figures 27 to 30 (abbreviated autorotation conversion) are for conversions in which the rotor speed was controlled aerodynamically from 0 to approximately 100 rpm with a subsequent controlled reduction in the rotor speed to 0 rpm. The data in figures 27 to 30 include the model angle of attack α, rotor collective and cyclic blade pitch angles A_0, A_1, B_1, and A_2, and the nondimensional steady forces and moments as a function of the rotor speed.

All conversions were performed with a tunnel dynamic pressure of approximately 7.2 lbf/ft^2 $\left(345 \text{ N/m}^2\right)$, resulting in a test Reynolds number of approximately 0.48×10^6 per ft $\left(1.6 \times 10^6 \text{ per meter}\right)$ (nonrotating).

COMMENTS

The control position data A_0 and A_1 (figs. 23 to 25 and 27 to 29) were obtained with the primary requirement that the rotor accelerate or decelerate at a given aircraft angle of attack. There was only secondary consideration given, in establishing the conversion control schedule with rotor speed, to obtaining a steady pitching or rolling moment of zero. In addition, the amplitude of the oscillatory moments during conversion (given in fig. 3 and table I) was unknown and the use of large-amplitude B_1 cyclic pitch to reduce the amplitude had not been identified at the time the data were obtained. Therefore, the data variations with rotor speed are considered as samples of the type of control used in conversion and the corresponding variation in the lift and moments.

REFERENCES

1. Hohenemser, Kurt H.: Remarks on Dynamic Problems of Composite Aircraft.
   J. Amer. Helicopter Soc., vol. 13, no. 1, Jan. 1968, pp. 11-13.

2. Huston, R. J.; and Shivers, J. P.: The Conversion of the Rotor/Wing Aircraft. Fluid
   Dynamics of Rotor and Fan Supported Aircraft at Subsonic Speeds, AGARD CP
   No. 22, Sept. 1967.

3. Mechtly, E. A.: The International System of Units — Physical Constants and Conver-
   sion Factors. NASA SP-7012, 1964.

4. Harned, M. S.; and Head, R. E.: Hot Cycle Rotor/Wing High-Speed VTOL Aircraft.
   Proceedings of 1st National V/STOL Aircraft Symposium, Amer. Helicopter Soc.,
   Inc., Nov. 1965, pp. I-29 - I-81.

5. Winston, Matthew W.; and Huston, Robert J.: Wind-Tunnel Investigation of Steady-
   State Aerodynamics of a Composite-Lift VTOL Aircraft Model. NASA TN D-5232,
   1969.

6. Anon.: Helicopter Flying and Ground Handling Qualities; General Requirements for.
   Mil. Specif. MIL-H-8501A, Sept. 7, 1961.

7. Anon.: Flying Qualities of Piloted Airplanes. Mil. Specif. MIL-F-8785 (ASG),
   Sept. 1, 1954.

8. Ward, John F.: Exploratory Flight Investigation and Analysis of Structural Loads
   Encountered by a Helicopter Hingeless Rotor System. NASA TN D-3676, 1966.
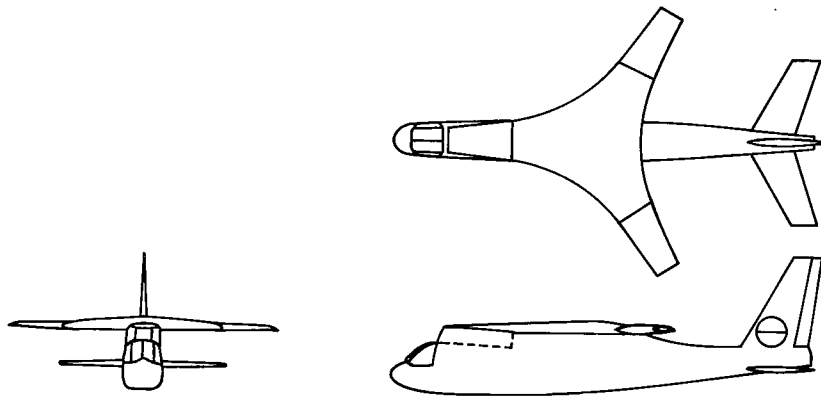
Figure 1.- Typical rotor/wing design.

HELICOPTER FLIGHT   AUTOGYRO FLIGHT   AIRPLANE
                                  AND   FLIGHT
                             CONVERSION
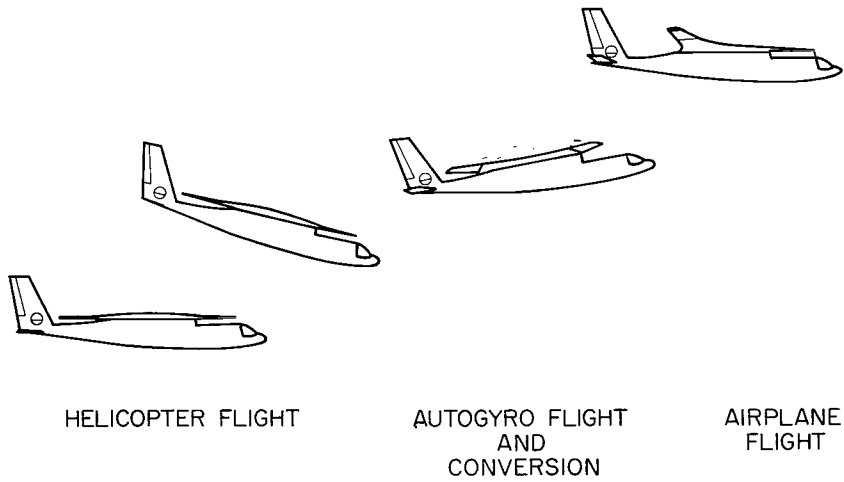
Figure 2.- Rotor/wing flight modes.
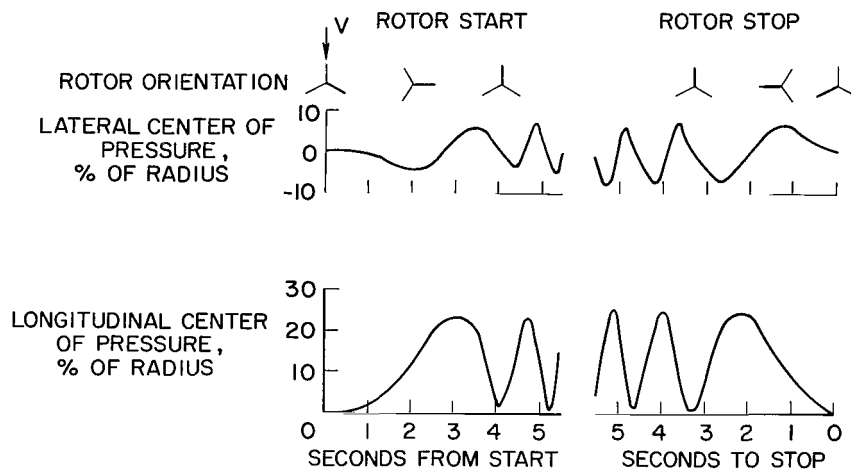
Figure 3.- Typical center-of-pressure movement from airplane condition during rotor starting and stopping.
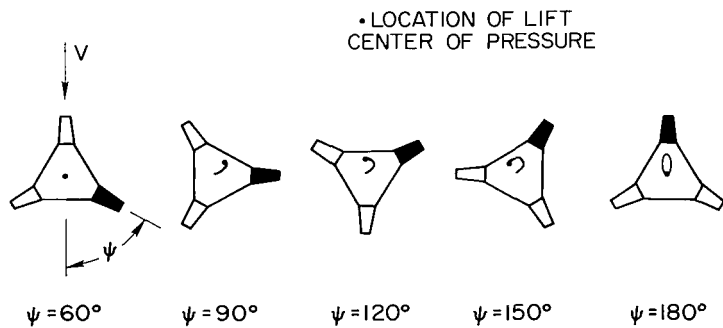
Figure 4.- Lift center-of-pressure motion during rotor revolution.
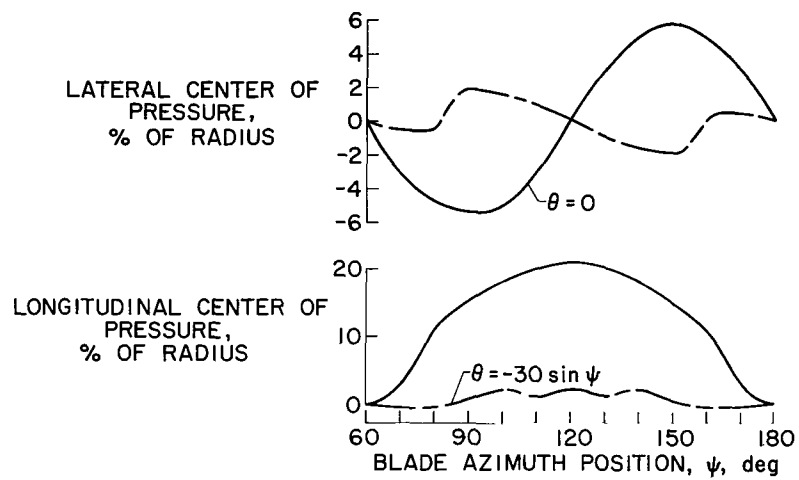
Figure 5.- Center-of-pressure movement from airplane condition during rotor revolution. Static model; configuration 2; $\alpha = 16°$.
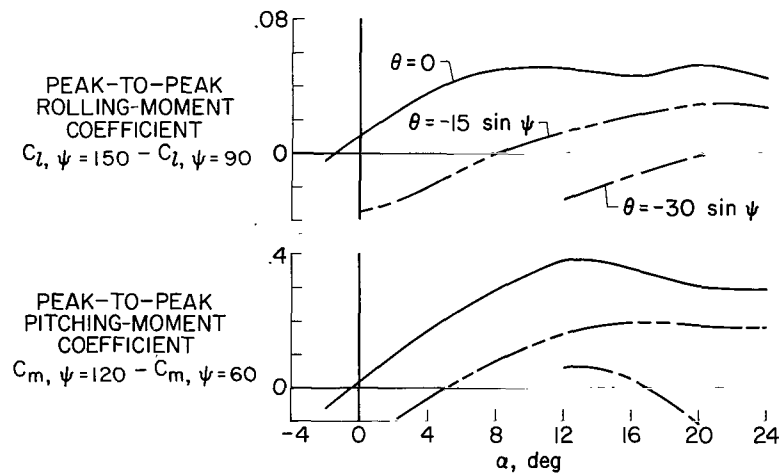
Figure 6.- Effect of angle of attack on moments during rotor revolution. Static model; configuration 2.
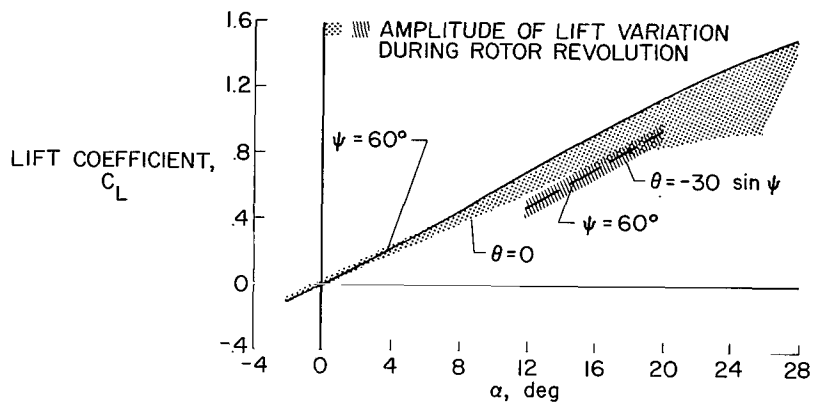
Figure 7.- Effect of large-amplitude cyclic pitch on lift. Static model; configuration 2.
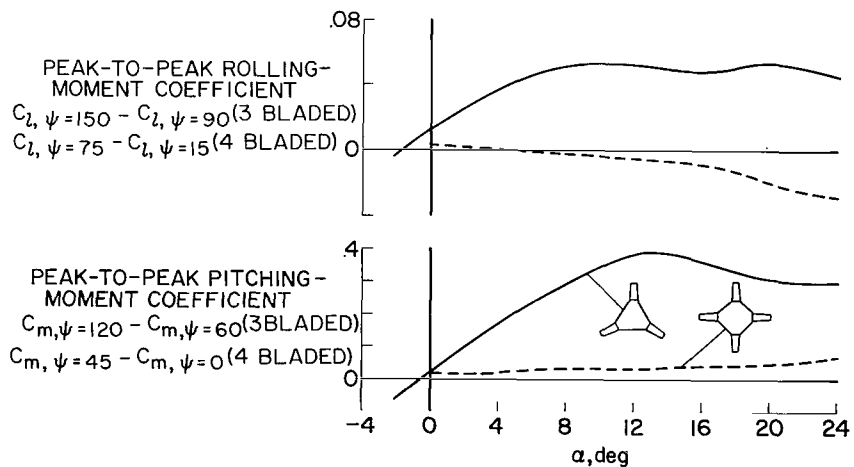
Figure 8.- Effect of number of blades on peak-to-peak moments during rotor revolution. Static models; $\theta = 0$.
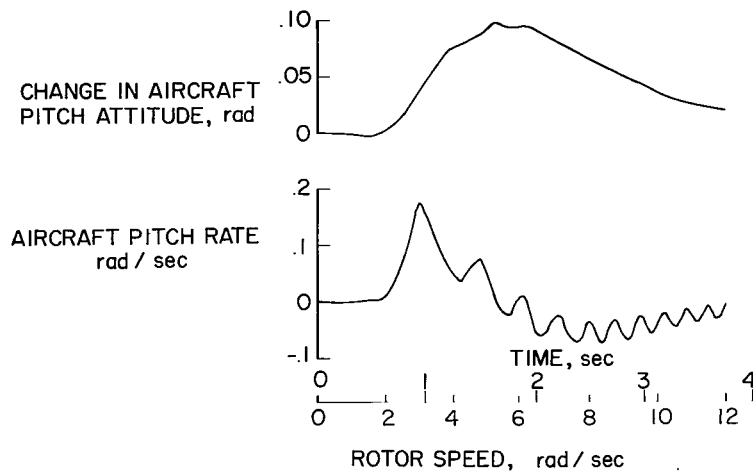
Figure 9.- Longitudinal response of rotor/wing with untrimmed center-of-pressure movement during rotor start.
$\dot{\Omega} = 3.2$ rad/sec^2; Airspeed = 150 knots.
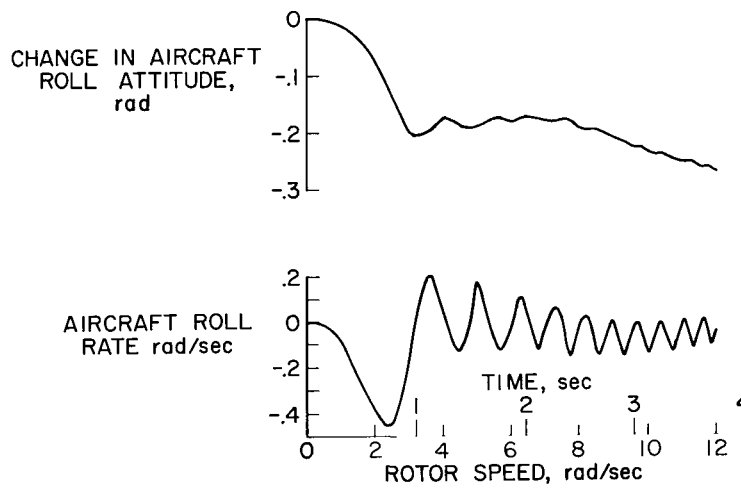
Figure 10.- Lateral response of rotor/wing with untrimmed center-of-pressure movement during rotor start.
$\dot{\Omega} = 3.2$ rad/sec^2.

30
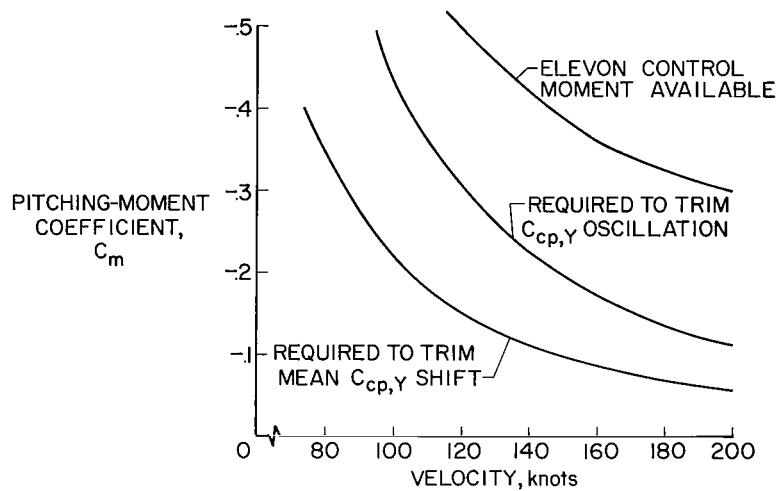
Figure 11.- Rotor/wing longitudinal control. $C_{cp,Y} = 12.5$.
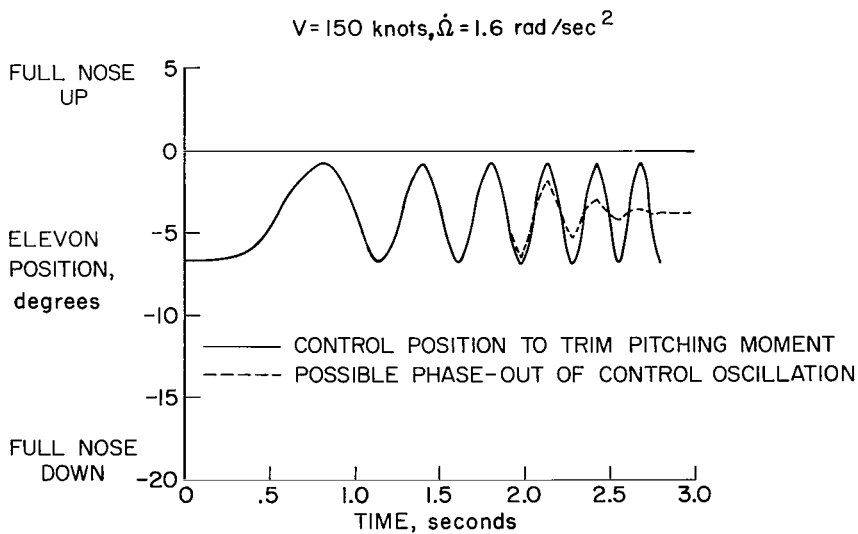
Figure 12.- Horizontal tail deflections to trim longitudinal center-of-pressure oscillations. $V = 150$ knots; $\dot{\Omega} = 3.2$ rad/sec^2; $C_{cp,Y} = 12.5$.
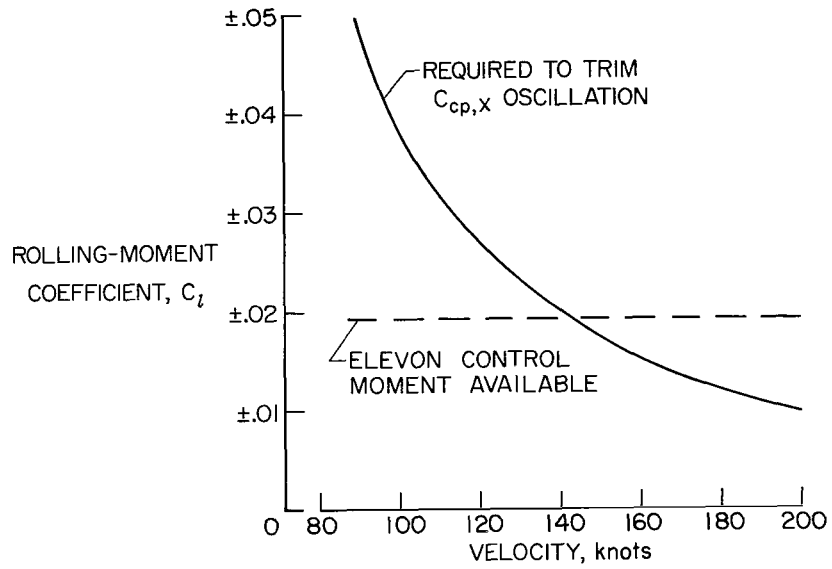
Figure 13.- Rotor/wing lateral control. $C_{cp,X} = 6.25.$
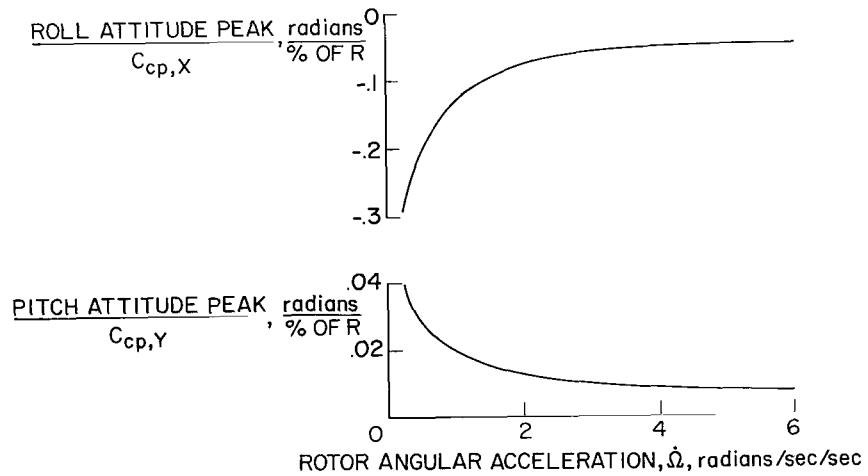
Figure 14.- Effect of rotor acceleration rate on disturbance amplitude during conversion. $V = 150$ knots; $x_{cg} - N_0 = 0.2$; decoupled between axes.

ROLL ATTITUDE PEAK , $\dfrac{\text{radians}}{\text{% OF R}}$

$C_{cp,X}$

0

-.1

-.2

-.3

PITCH ATTITUDE PEAK, $\dfrac{\text{radians}}{\text{% OF R}}$

$C_{cp,Y}$

.04

.02

0   80   100   120   140   160   180   200

CONVERSION AIRSPEED , knots
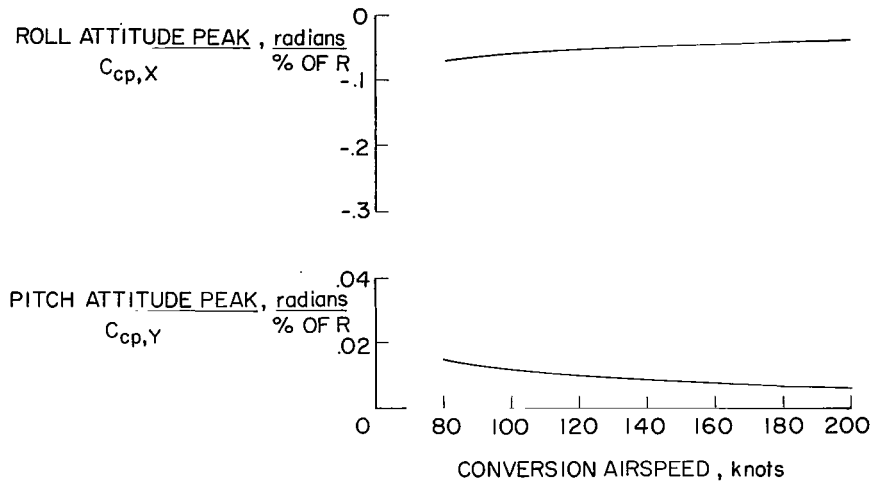
Figure 15.- Effect of airspeed on disturbance amplitude during conversion.
$\dot{\Omega} = 3.2$ rad/sec^2; $x_{cg} - N_0 = 0.2$; decoupled.

ROLL ATTITUDE PEAK , $\dfrac{\text{radians}}{\text{% OF R}}$

$C_{cp,X}$

ZERO ROTOR DAMPING $x_{cg} - N_0 = 0.20$

0

-.1   NO EFFECT,
                       NOT COUPLED

-.2

-.3

PITCH ATTITUDE PEAK , $\dfrac{\text{radians}}{\text{% OF R}}$

$C_{cp,Y}$

.04

.02

0   .30   0   50 %

$x_{cg} - N_0$ ASSUMED ROTOR
                        DAMPING
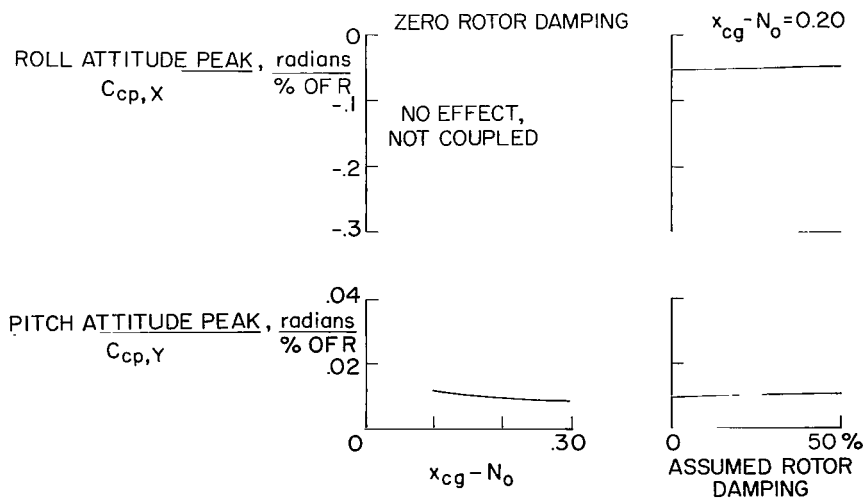
Figure 16.- Effect of static margin and additional rotor damping on disturbance amplitude during conversion.
$V = 150$ knots; $\dot{\Omega} = 3.2$ rad/sec^2.

33

ft

0	1	2	3	4

0	0.5	1.0
m

Rotor
center
of
rotation

Reference center of gravity
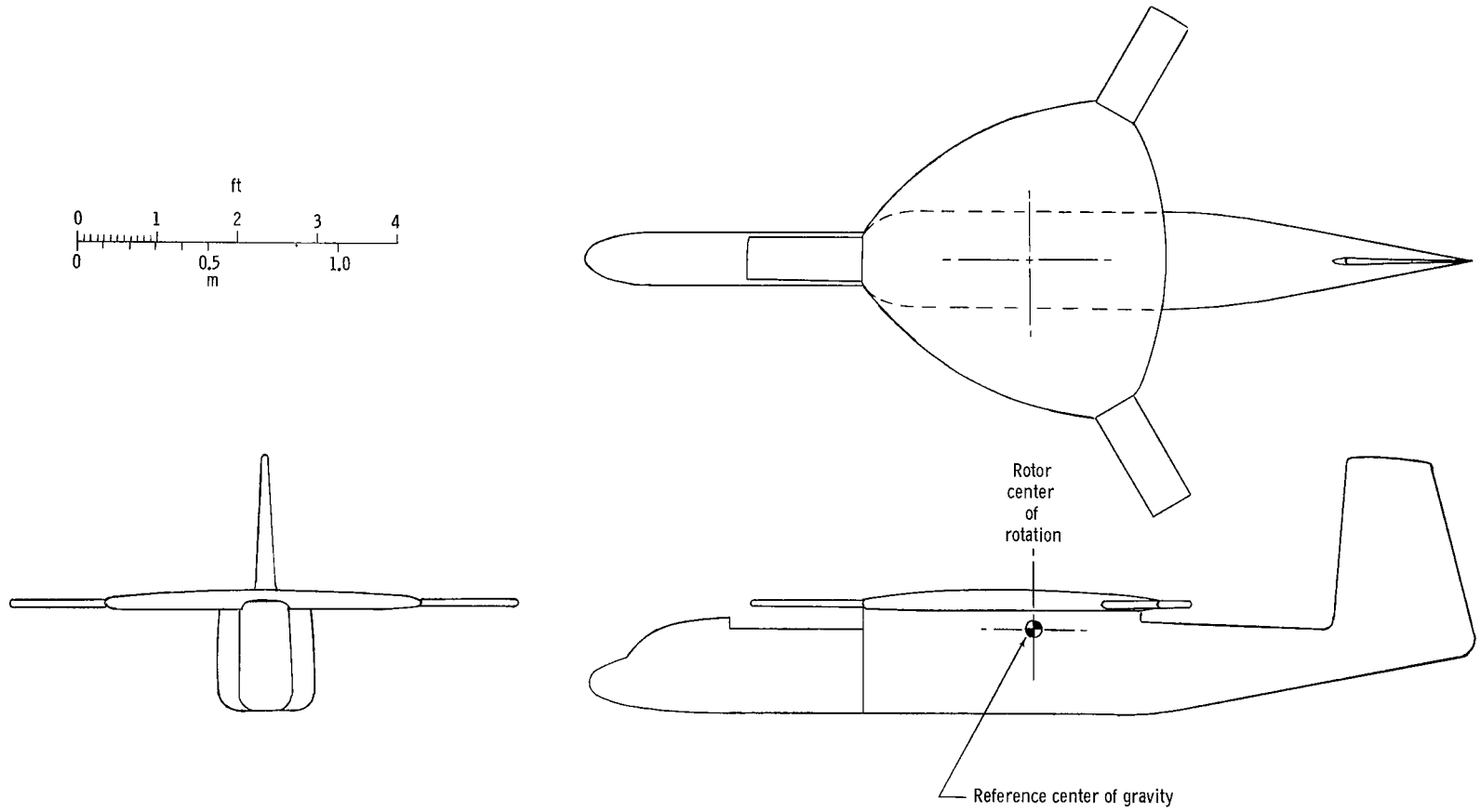
(a) Three-view drawing of model (rotor configuration 1).

Figure 17.- Rotor/wing model.

ft
0   1   2   3   4

0   0.5   1.0
m
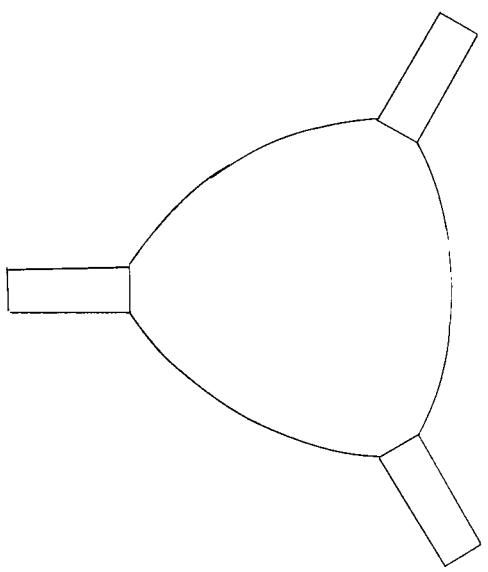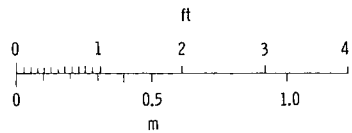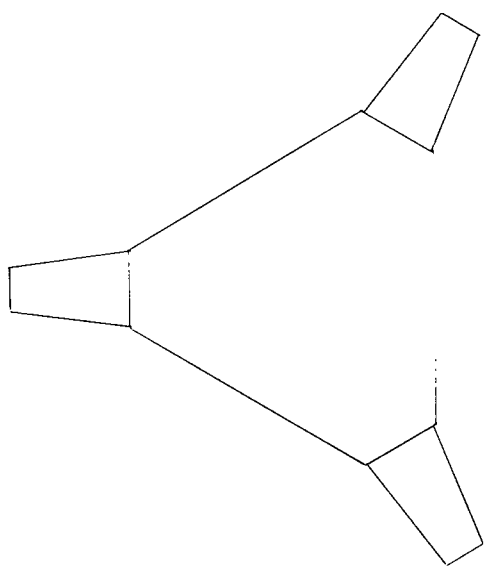
Configuration 1

Configuration 2
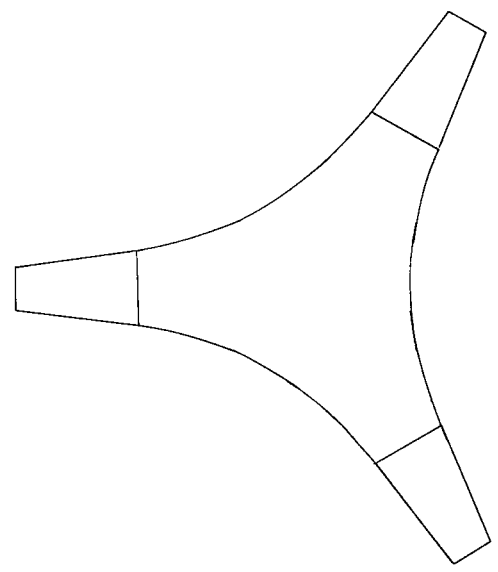
Configuration 3

(b) Plan views of rotor configurations.

Figure 17.- Concluded.
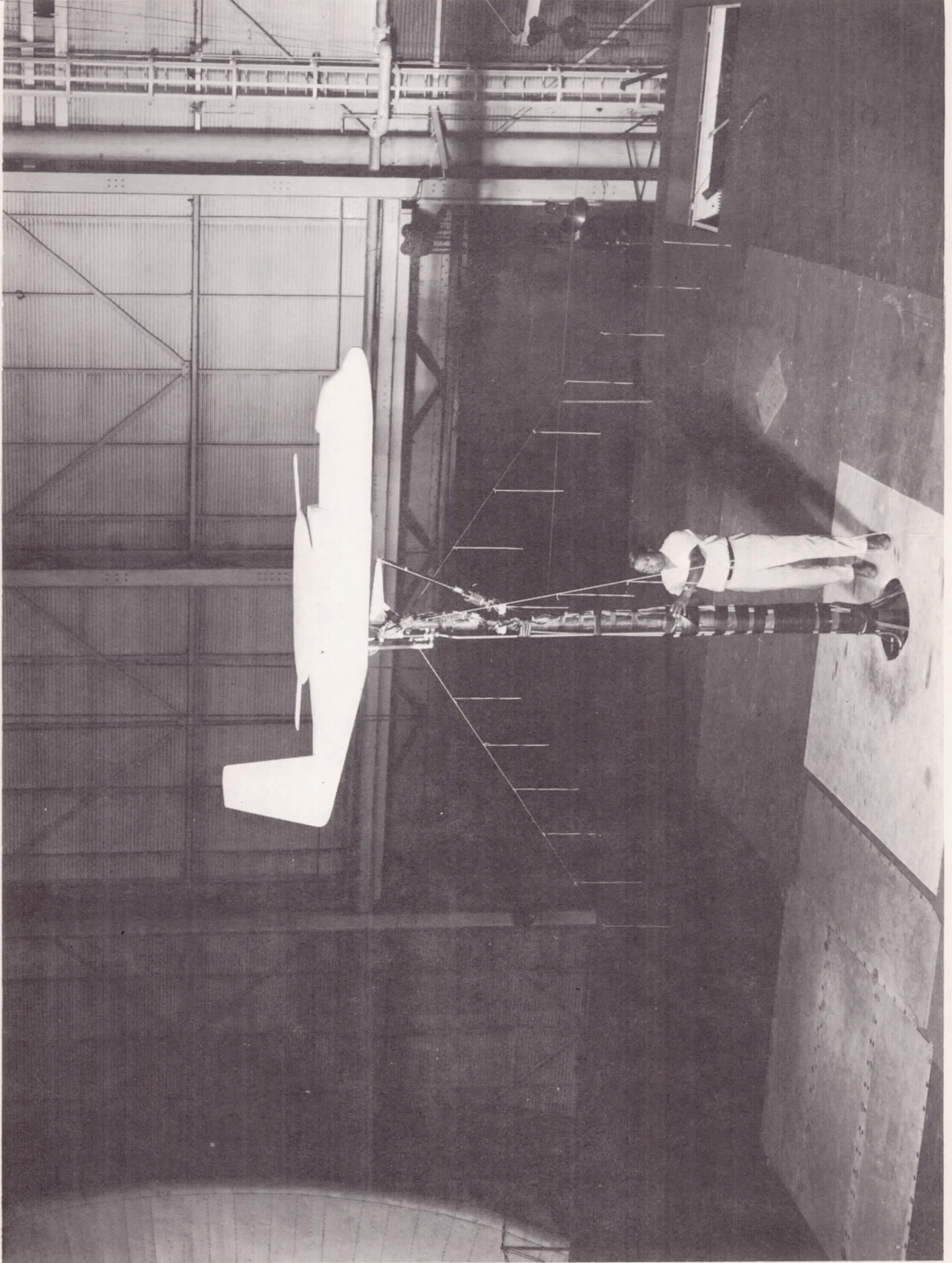
Figure 18.- Model installed in Langley full-scale tunnel.
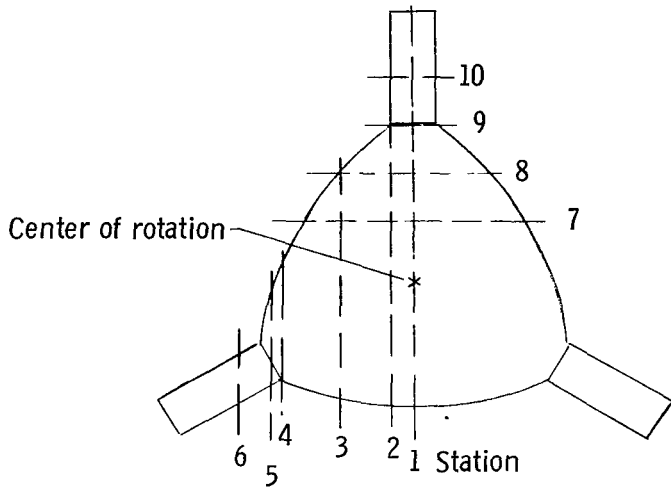
Station location from center of
rotation, radial or lateral distance,
$\psi = 60°$

Sta.	Inches	Centimeters
1	0	0
2	5. 18	13. 16
3	12. 82	32. 56
4	17. 95	45. 59
5	22. 20	56. 39
6	29. 56	75. 08
7	9. 83	24. 97
8	17. 20	43. 69
9	24. 57	62. 41
10	30. 00	76. 20
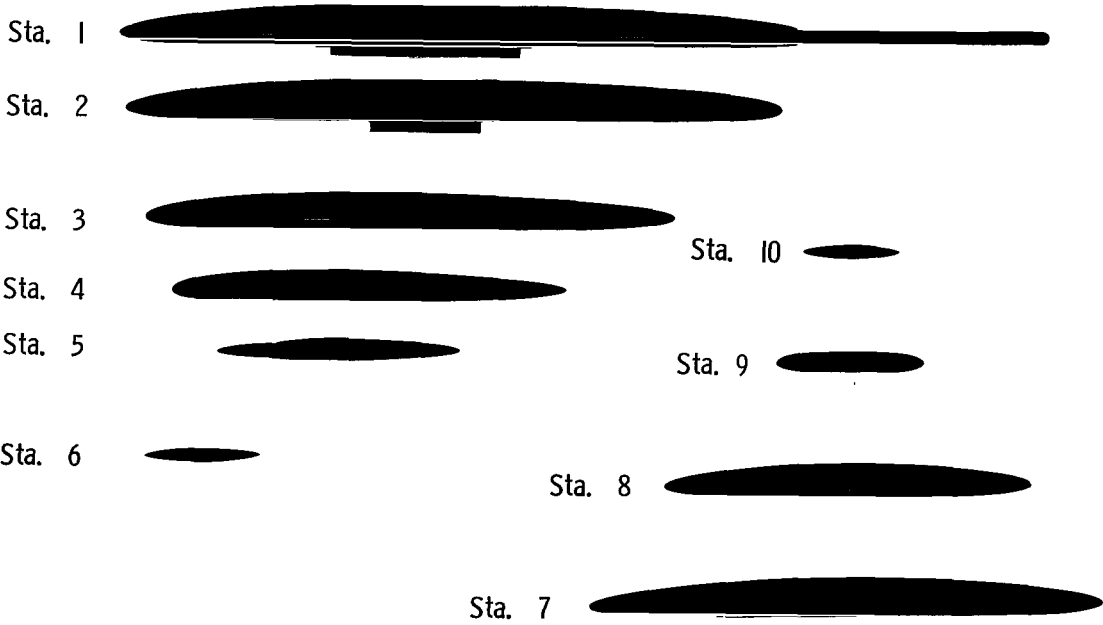
Figure 19.- Silhouettes of representative sections of the wing and rotor of the rotor/wing configuration 1.
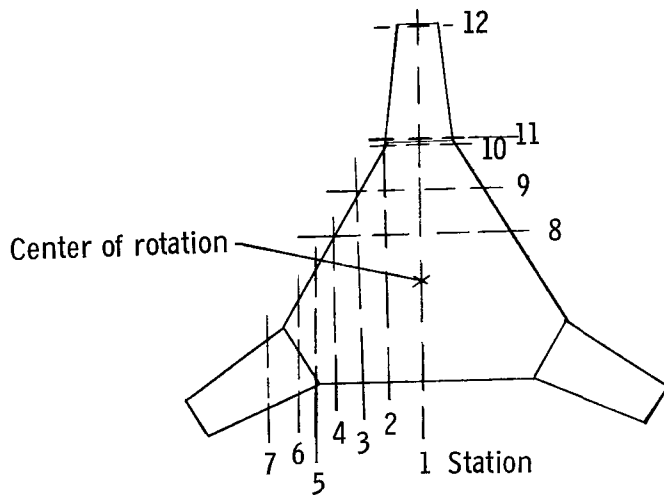
37

Station location from center of rotation, radial or lateral distance, $\psi = 60°$

Sta.	Inches	Centimeters
1	0	0
2	6.21	15.77
3	11.00	27.96
4	15.50	39.37
5	19.50	49.53
6	22.00	55.88
7	26.75	67.95
8	8.70	22.10
9	16.53	41.99
10	24.36	61.87
11	26.36	66.95
12	41.95	106.54
	(1 from tip)	(2.54 from tip)

Center of rotation

1 Station

Sta. 1
Sta. 2
Sta. 3
Sta. 4
Sta. 5
Sta. 6
Sta. 7

Sta. 12
Sta. 11
Sta. 10
Sta. 9
Sta. 8
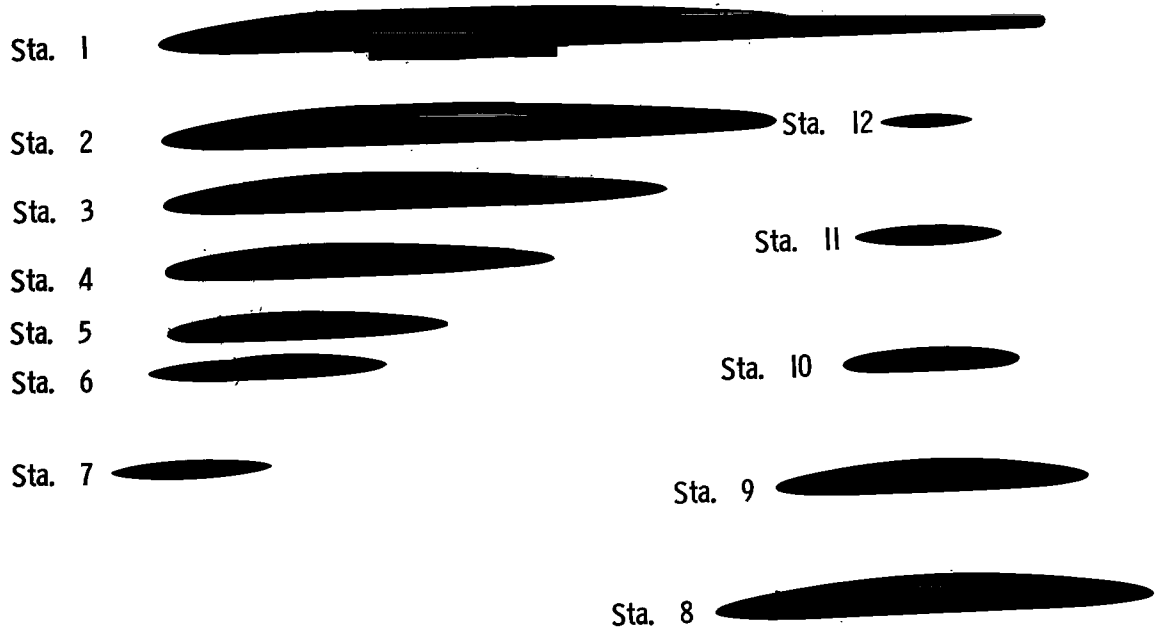
Figure 20.- Silhouettes of representative sections of the wing and rotor of the rotor/wing configuration 2.
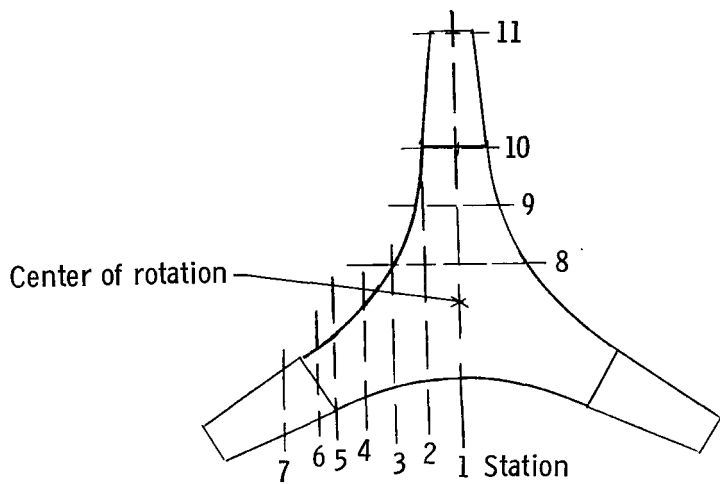
Station location from center of
rotation, radial or lateral dis-
tance, $\psi = 60°$

Sta.	Inches	Centimeters
1	0	0
2	5.43	13.79
3	11.68	29.67
4	15.68	39.83
5	19.50	49.53
6	22.00	55.88
7	26.75	67.95
8	6.68	16.97
9	15.50	39.37
10	24.56	62.38
11	41.95	106.54
	(1 from tip)	(2.54 from tip)
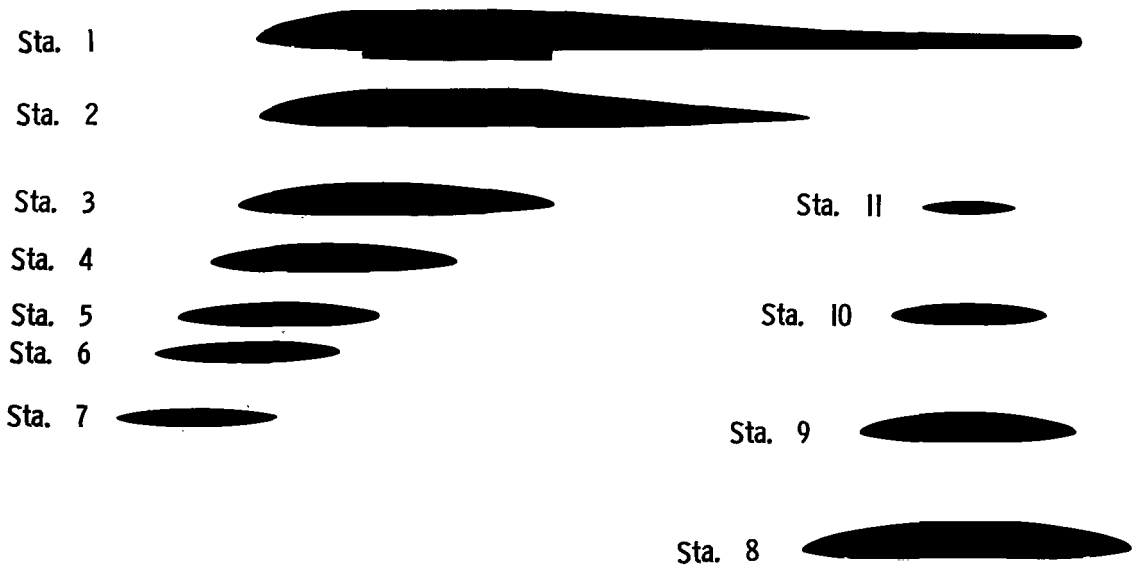
Figure 21.- Silhouettes of representative sections of the wing and rotor of the rotor/wing configuration 3.
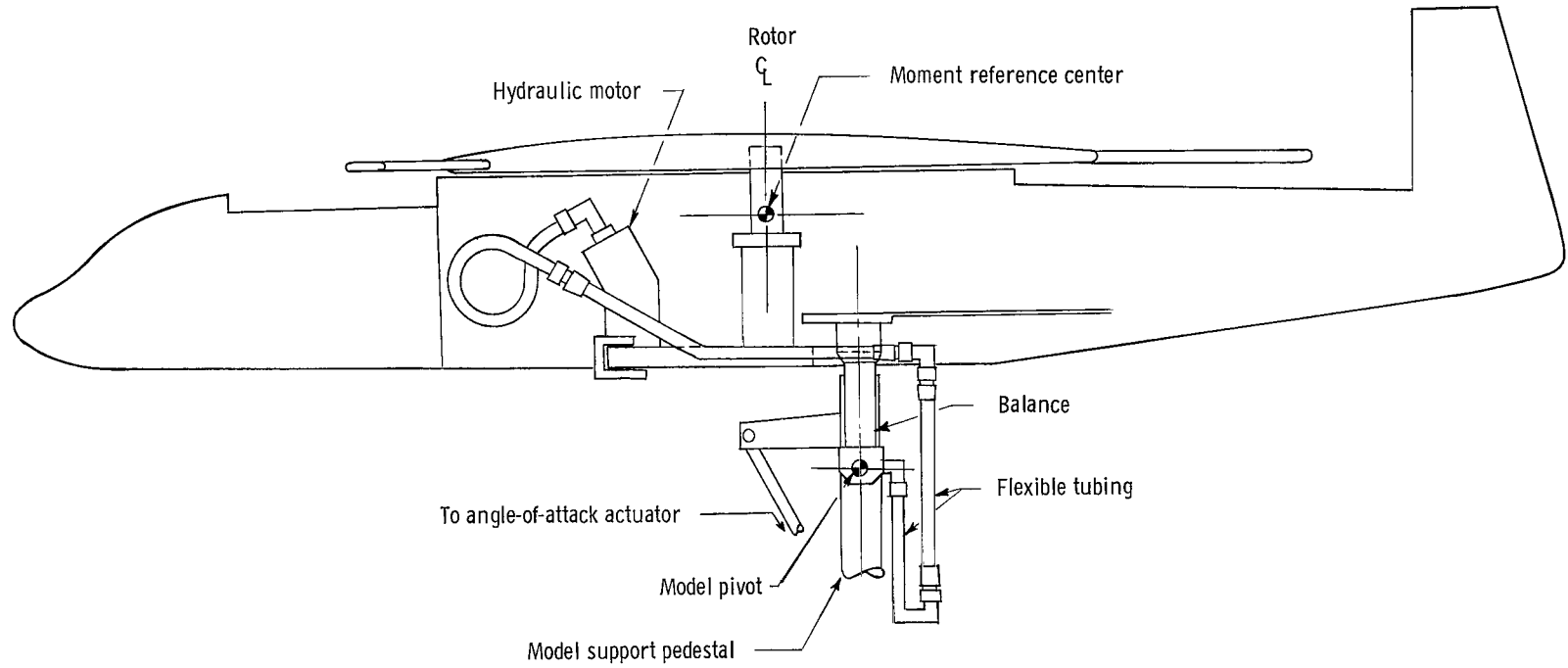
Figure 22.- Model mounting system, balance installation, and hydraulic drive motor arrangement.
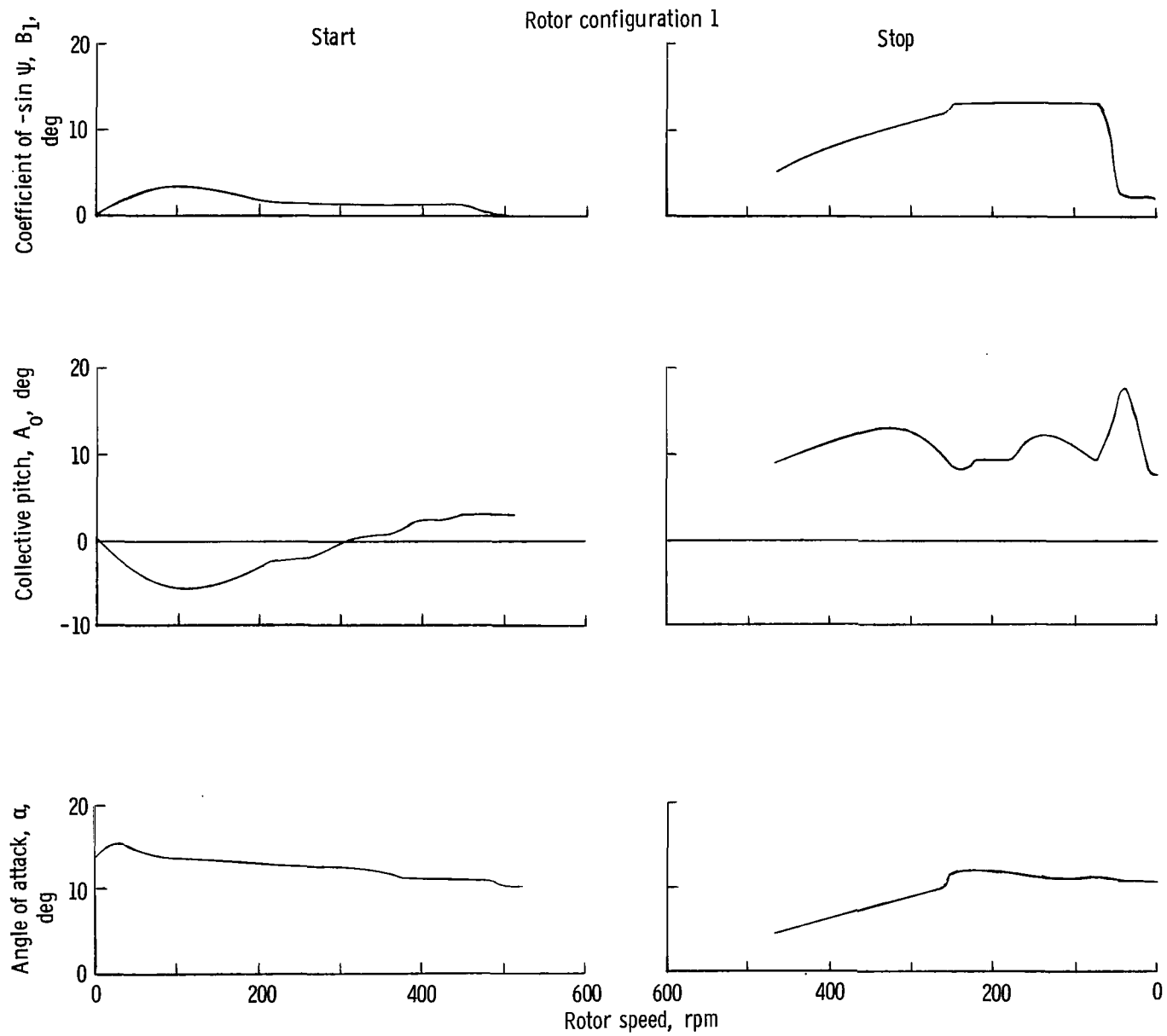
Figure 23.- Aircraft characteristics during complete autorotation conversion with rotor configuration 1. $A_1 = 0$; $A_2 = 2.5^0$.
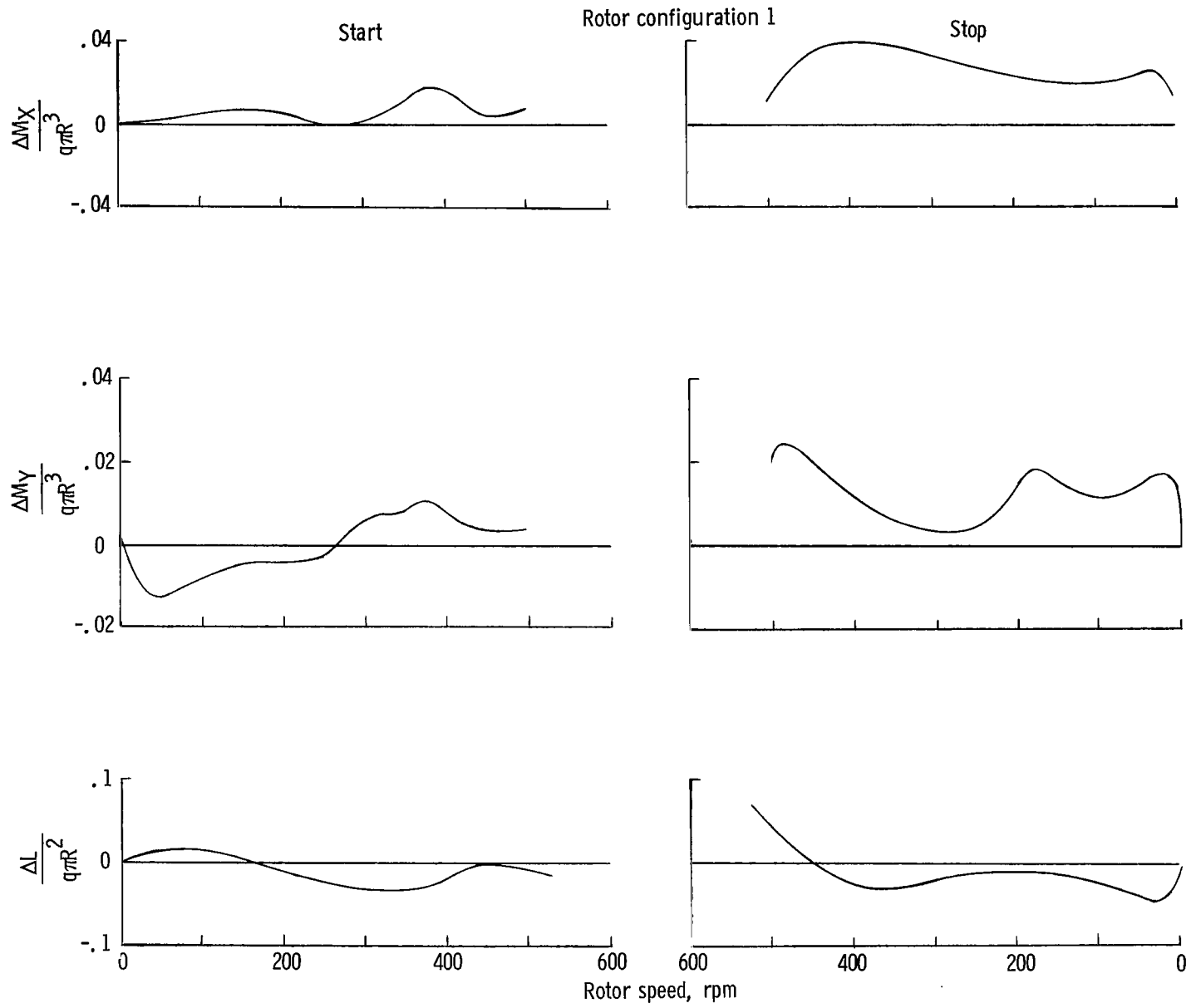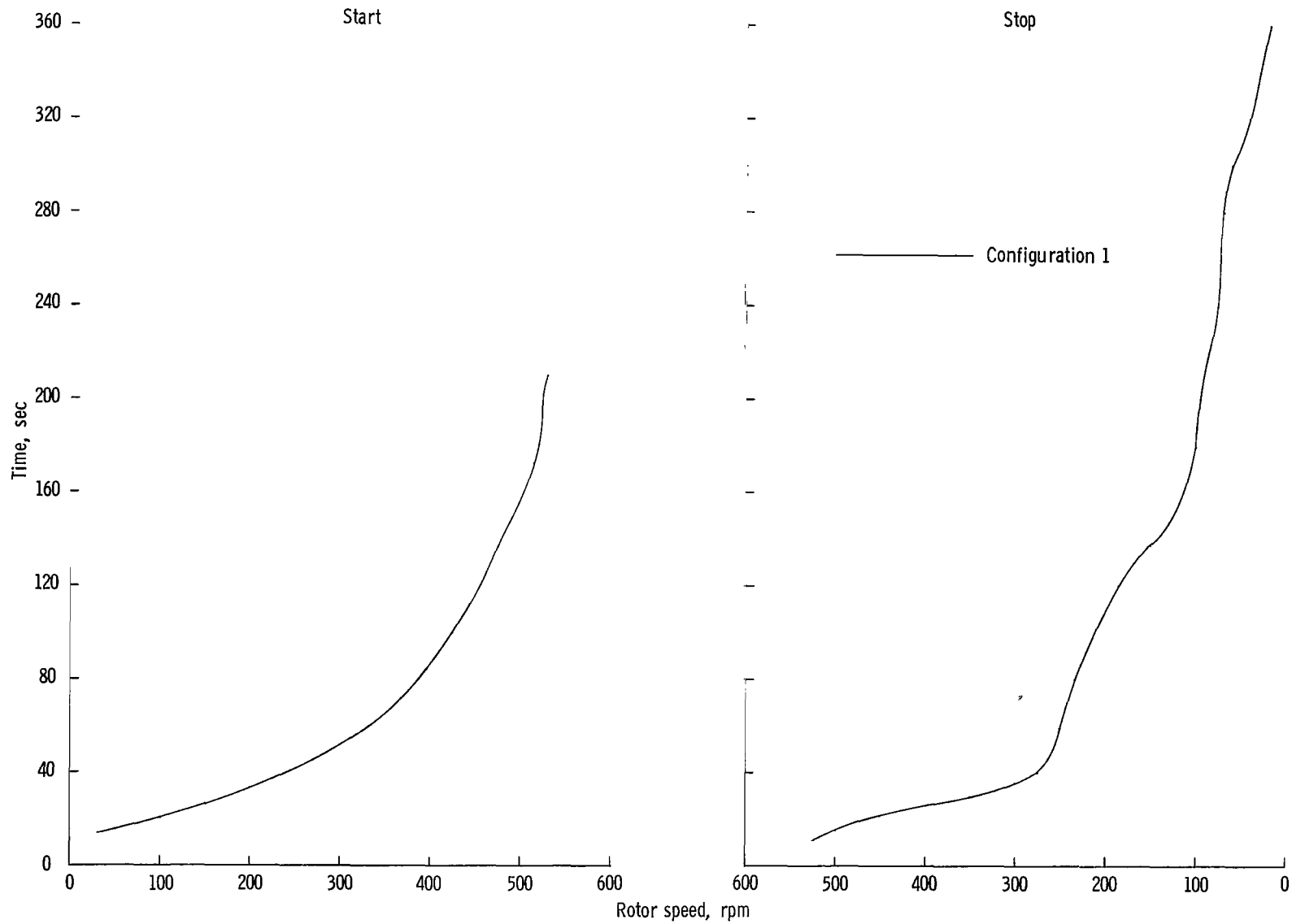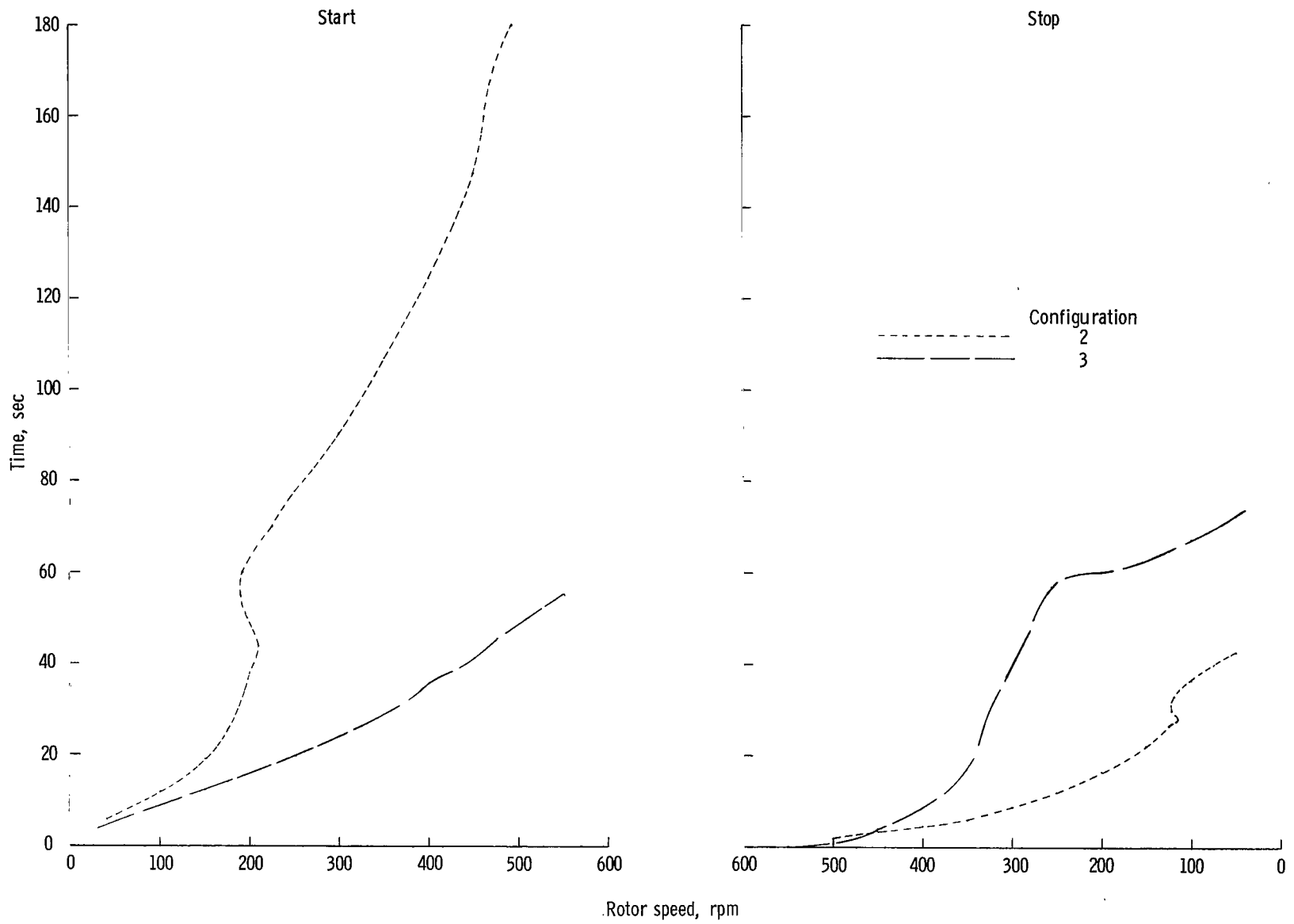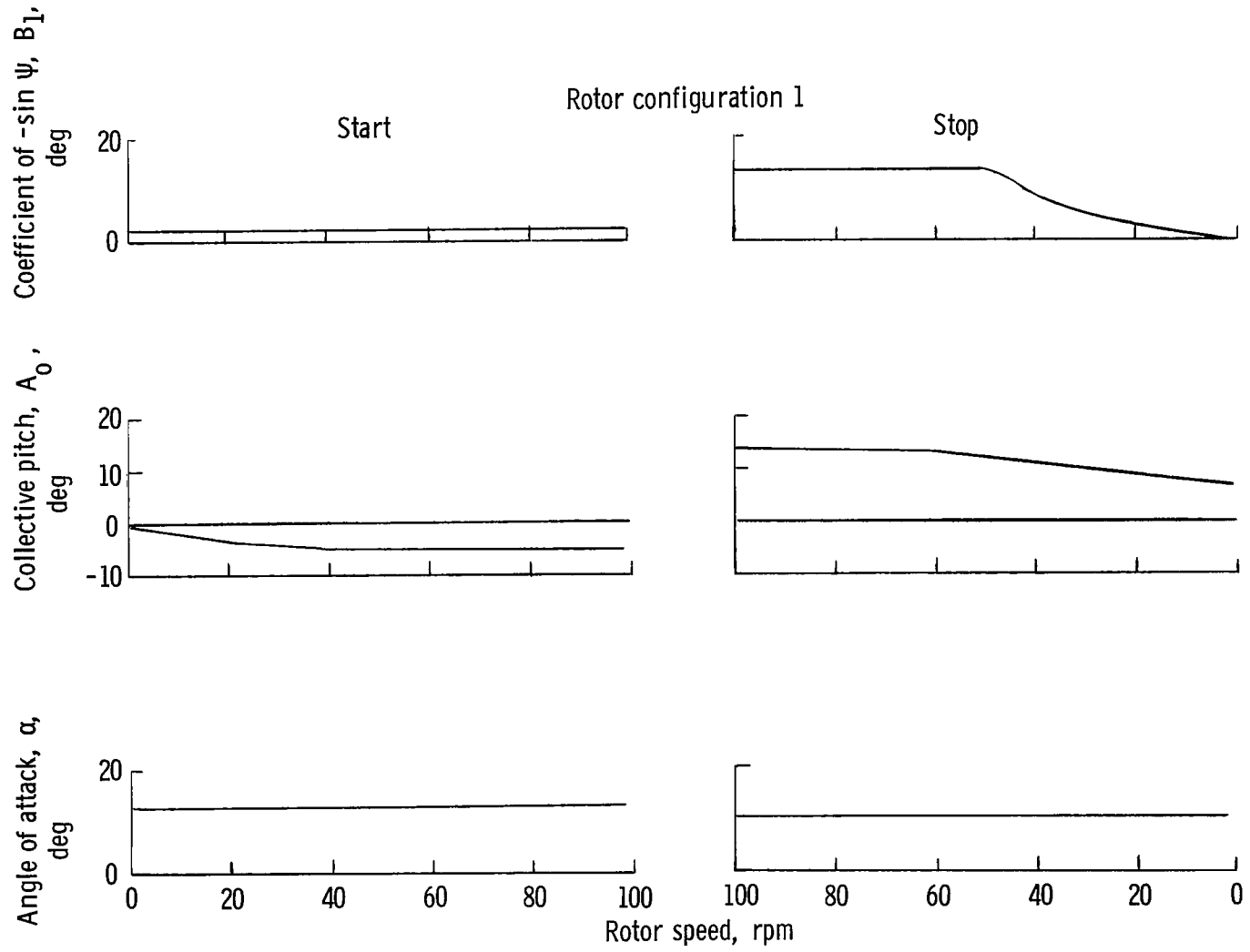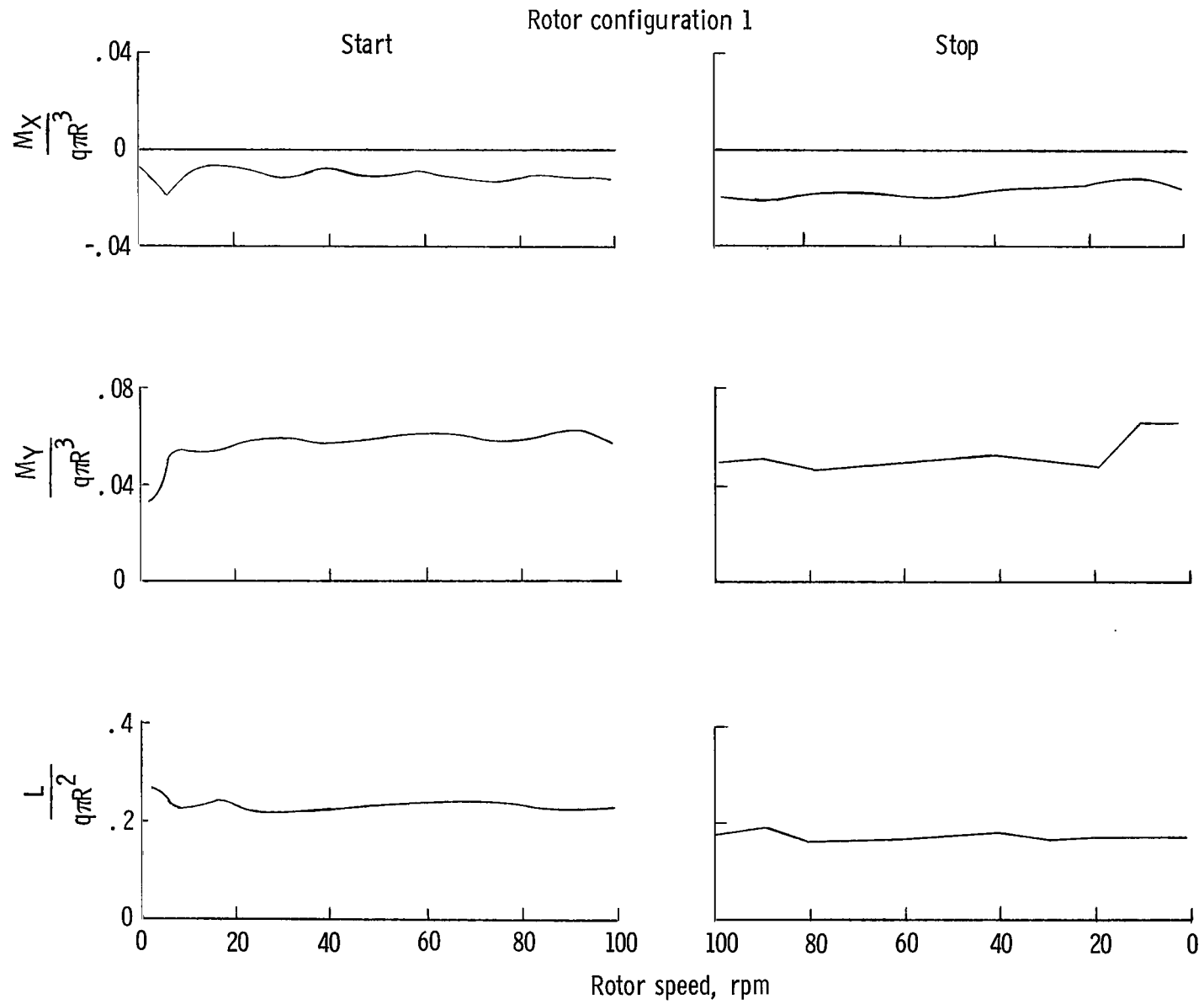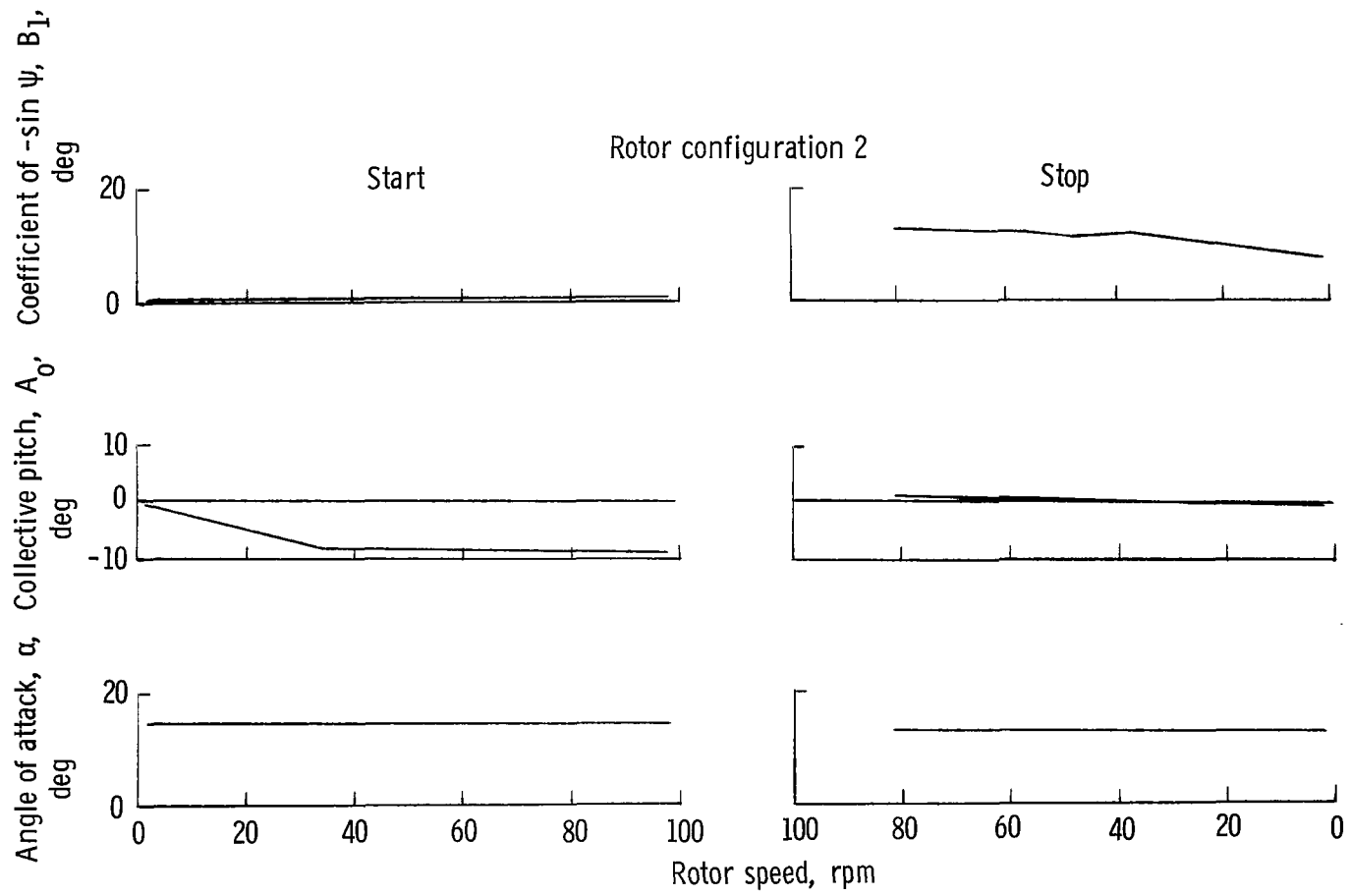
Figure 23.- Concluded.
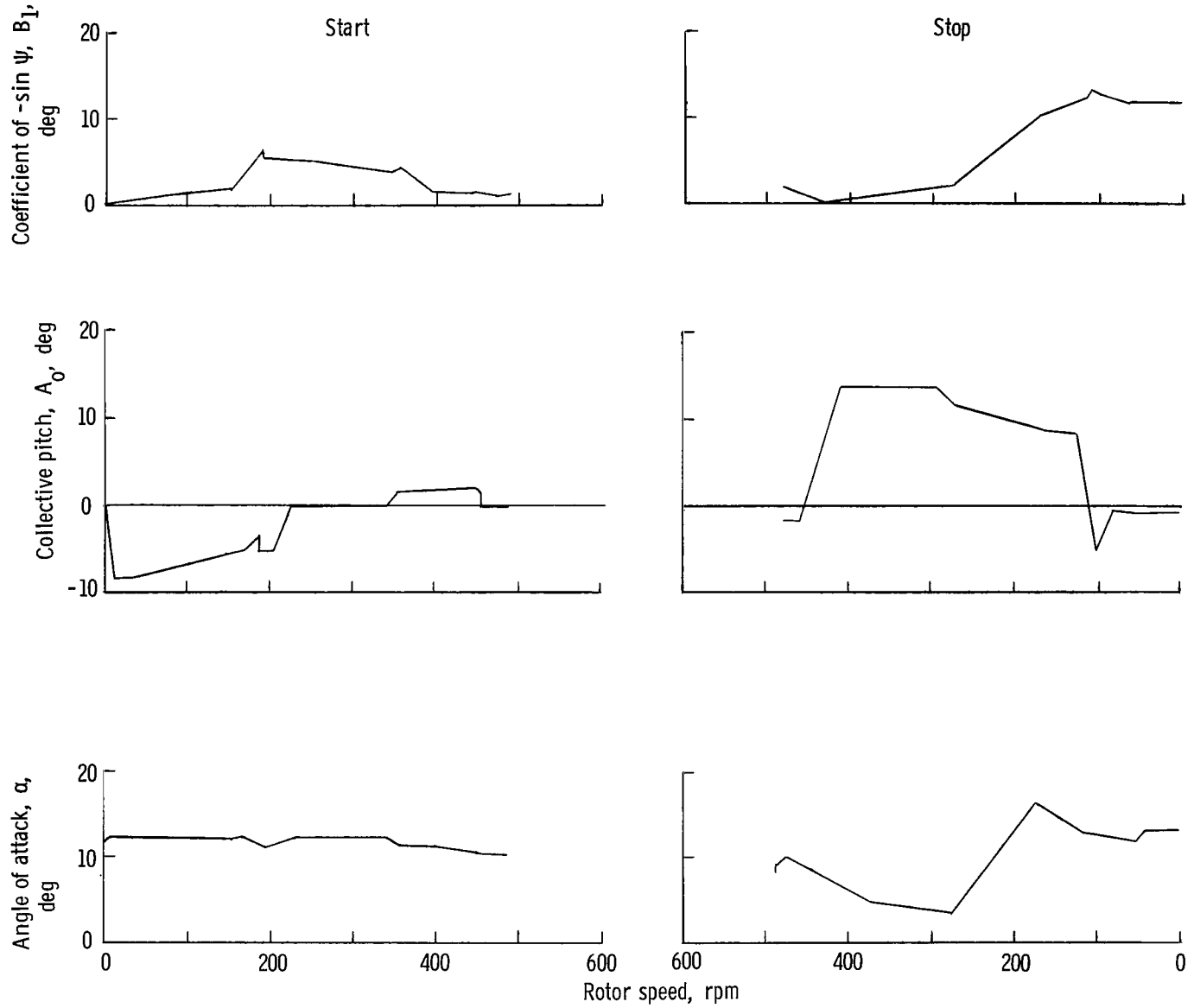
Figure 24.- Aircraft characteristics during complete autorotation conversion with rotor configuration 2. $A_1 = 0$; $A_2 = 2.5°$.

Rotor configuration 2
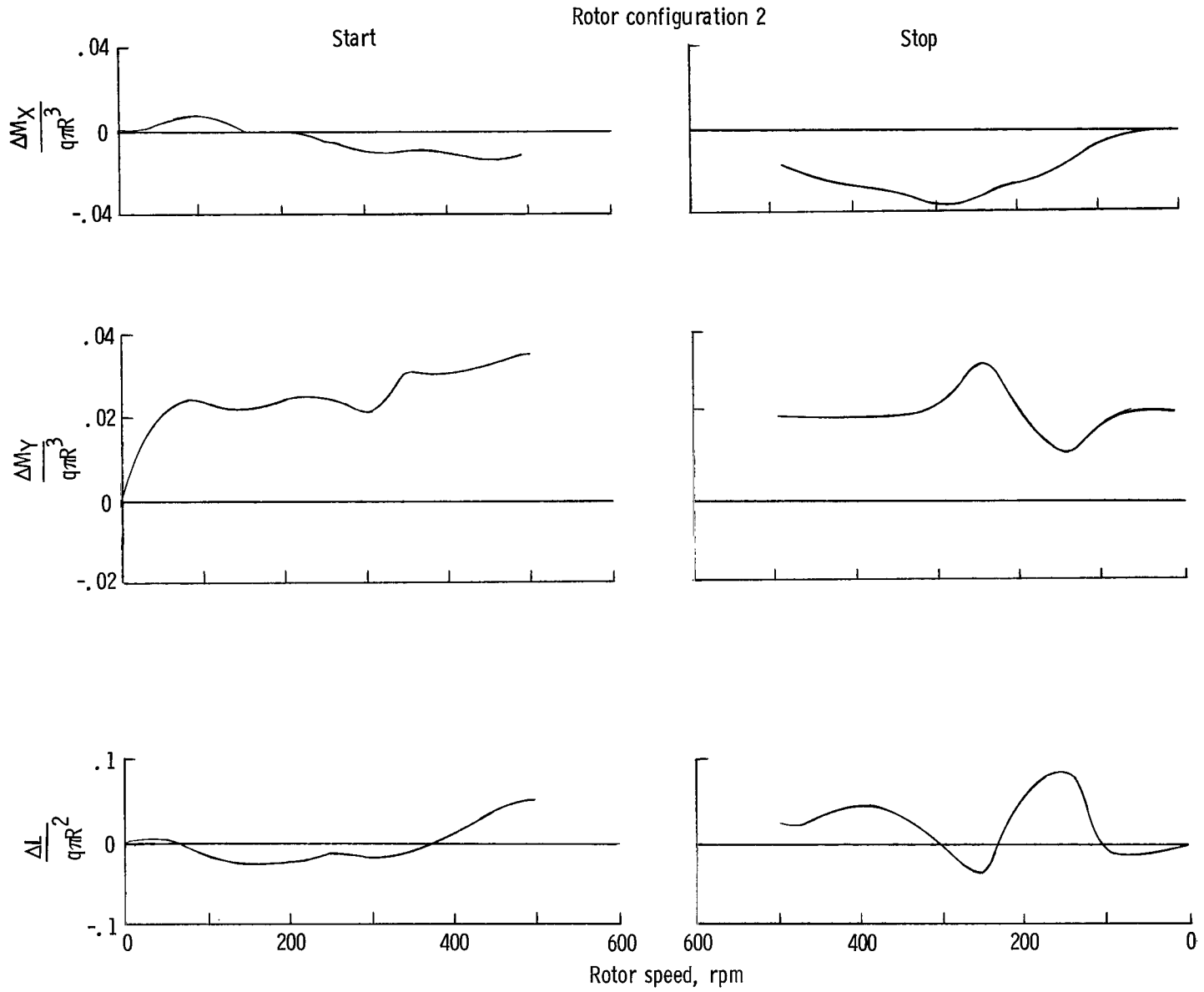
Figure 24.- Concluded.

Figure 25.- Aircraft characteristics during complete autorotation conversion with rotor configuration 3. $A_1 = 0$; $A_2 = 2.5^0$.

Rotor configuration 3

Start

Stop

$\dfrac{\Delta M_X}{q\pi R^3}$

.04

0

-.04

$\dfrac{\Delta M_Y}{q\pi R^3}$

.04

.02

0

-.02

$\dfrac{\Delta L}{q\pi R^2}$

.1

0

-.1

0   200   400   600

600   400   200   0
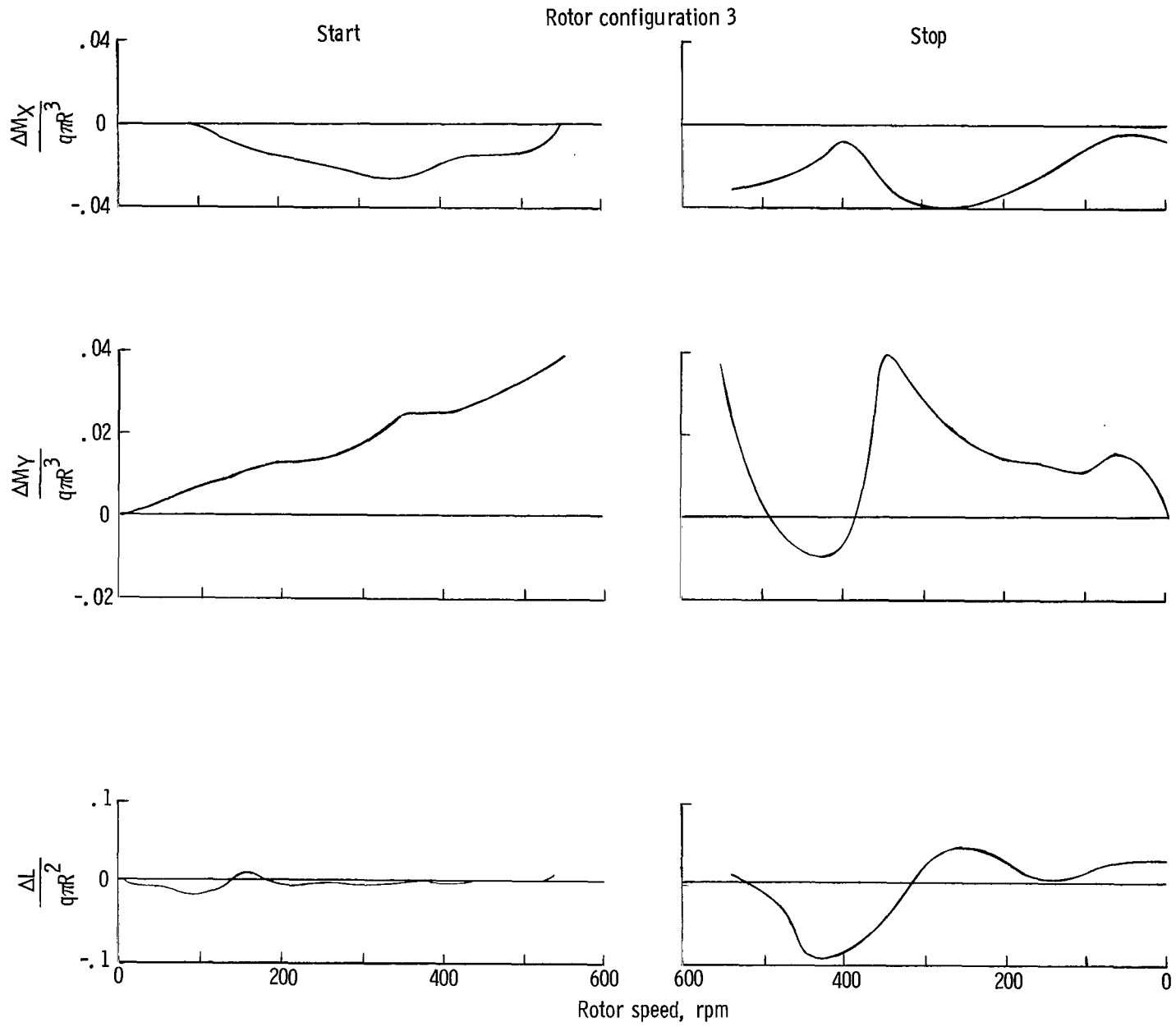
Rotor speed, rpm

Figure 25.- Concluded.

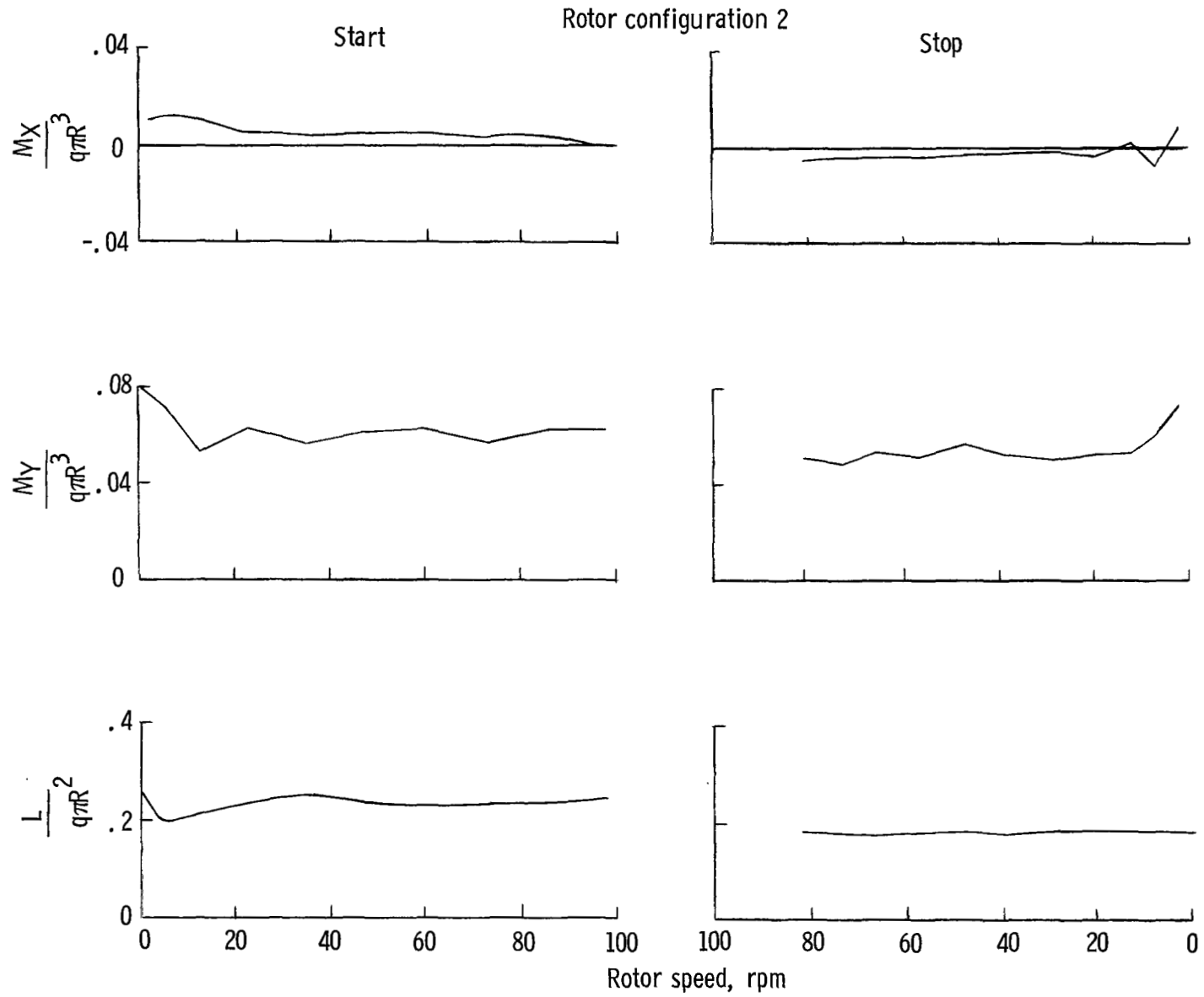Figure 26.- Variation of rotor speed with time during complete autorotation conversion. $A_1 = 0$; $A_2 = 2.5^0$.

Figure 26.- Concluded.

Figure 27.- Aircraft characteristics during abbreviated autorotation conversion with rotor configuration 1. $A_1 = 0$; $A_2 = 2.5^0$.

Rotor configuration 1

Figure 27.- Concluded.

Figure 28.- Aircraft characteristics during abbreviated autorotation conversion with rotor configuration 2. $A_1 = 0$; $A_2 = 2.5°$.
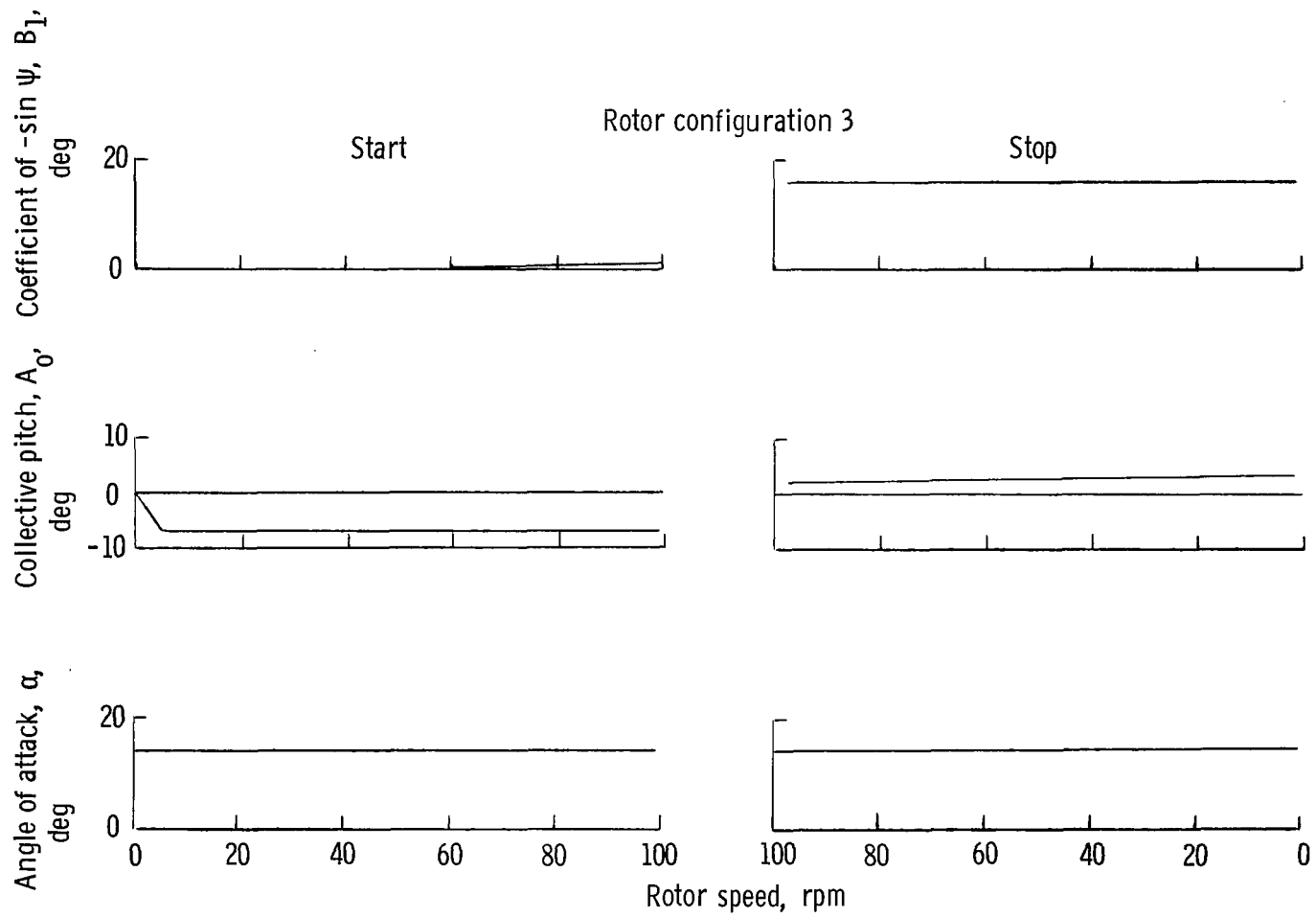
Figure 28.- Concluded.

Figure 29.- Aircraft characteristics during abbreviated autorotation conversion with rotor configuration 3. $A_1 = 0$; $A_2 = 2.5°$.

Rotor configuration 3
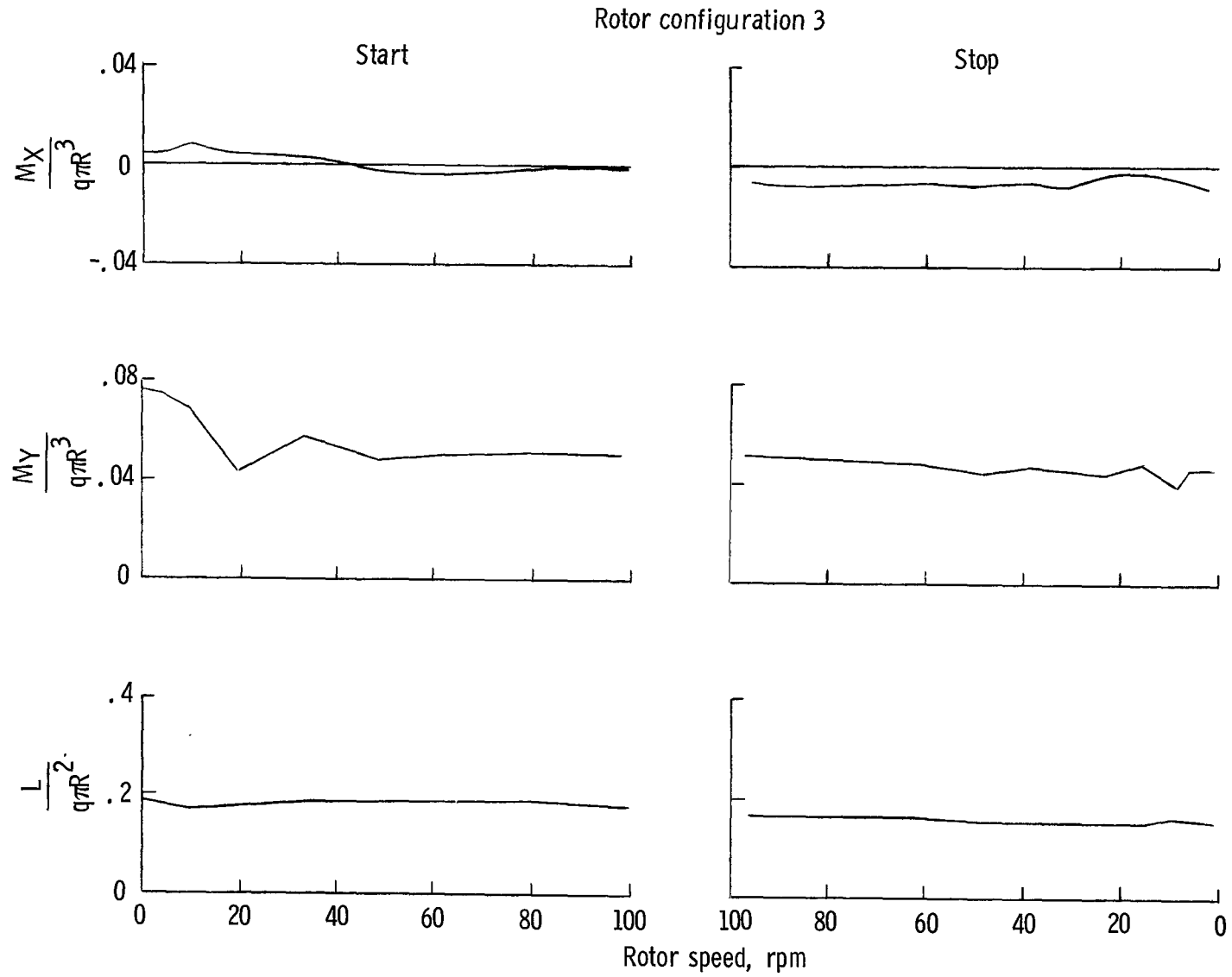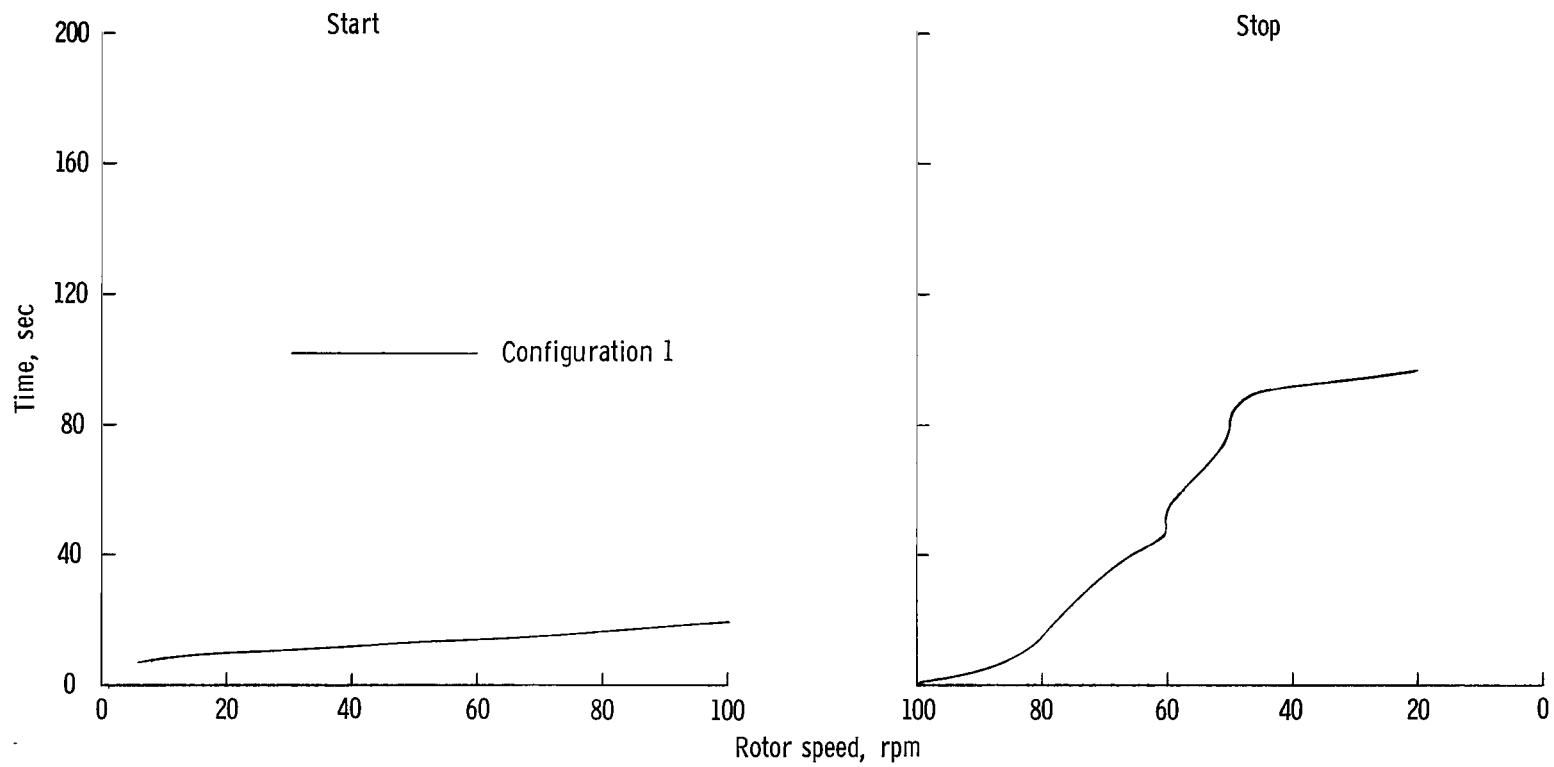

Figure 29.- Concluded.

Figure 30.- Variation of rotor speed with time during abbreviated autorotation conversion. $A_1 = 0$; $A_2 = 2.5^0$.
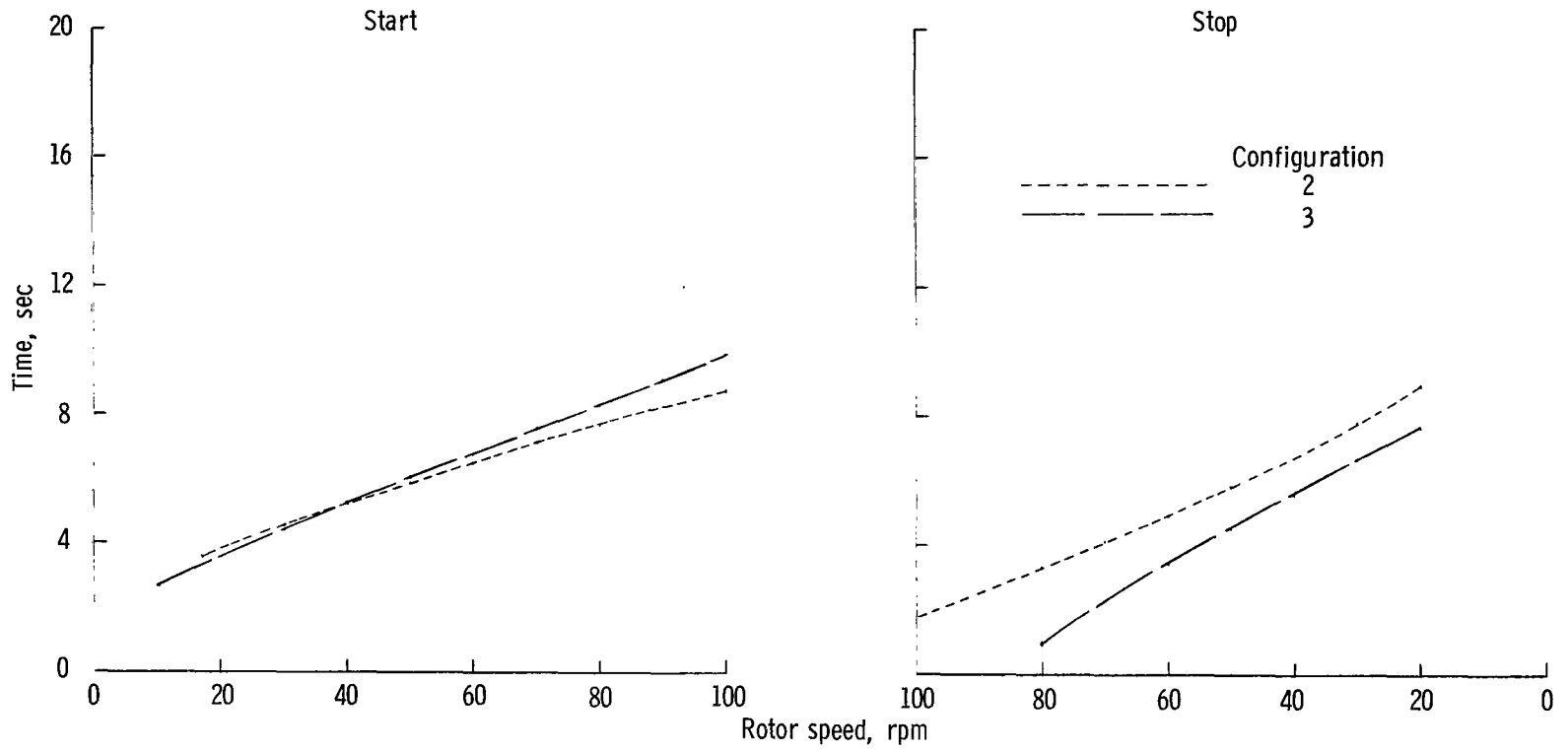
Figure 30.- Concluded.

FIRST CLASS MAIL

POSTAGE AND FEES PAID
NATIONAL AERONAUTICS AND
SPACE ADMINISTRATION

POSTMASTER: If Undeliverable (Section 158 Postal Manual) Do Not Return

"The aeronautical and space activities of the United States shall be conducted so as to contribute . . . to the expansion of human knowledge of phenomena in the atmosphere and space. The Administration shall provide for the widest practicable and appropriate dissemination of information concerning its activities and the results thereof."

— NATIONAL AERONAUTICS AND SPACE ACT OF 1958

NASA SCIENTIFIC AND TECHNICAL PUBLICATIONS

TECHNICAL REPORTS: Scientific and technical information considered important, complete, and a lasting contribution to existing knowledge.

TECHNICAL NOTES: Information less broad in scope but nevertheless of importance as a contribution to existing knowledge.

TECHNICAL MEMORANDUMS: Information receiving limited distribution because of preliminary data, security classification, or other reasons.

CONTRACTOR REPORTS: Scientific and technical information generated under a NASA contract or grant and considered an important contribution to existing knowledge.

TECHNICAL TRANSLATIONS: Information published in a foreign language considered to merit NASA distribution in English.

SPECIAL PUBLICATIONS: Information derived from or of value to NASA activities. Publications include conference proceedings, monographs, data compilations, handbooks, sourcebooks, and special bibliographies.

TECHNOLOGY UTILIZATION PUBLICATIONS: Information on technology used by NASA that may be of particular interest in commercial and other non-aerospace applications. Publications include Tech Briefs, Technology Utilization Reports and Notes, and Technology Surveys.

Details on the availability of these publications may be obtained from:

SCIENTIFIC AND TECHNICAL INFORMATION DIVISION

NATIONAL AERONAUTICS AND SPACE ADMINISTRATION
Washington, D.C. 20546